Author Manuscript

Author Manuscript

Author Manuscript

Author Manuscript

HHS Public Access

Author manuscript

Nature. Author manuscript; available in PMC 2020 December 24.

Published in final edited form as:

Nature. 2020 August ; 584(7820): 304–309. doi:10.1038/s41586-020-2452-0.

Structure of human $GABA_B$ receptor in an inactive state

Jinseo Park[1,19], **Ziao Fu**[2,19], **Aurel Frangaj**[1,19], **Jonathan Liu**[1,19], **Lidia Mosyak**[1,19], **Tong Shen**[3,19], **Vesna N. Slavkovich**[4], **Kimberly M. Ray**[1], **Jaume Taura**[5], **Baohua Cao**[1], **Yong Geng**[1,6], **Hao Zuo**[1], **Yongjun Kou**[6], **Robert Grassucci**[2], **Shaoxia Chen**[7], **Zheng Liu**[2], **Xin Lin**[8,14], **Justin P. Williams**[9], **William J. Rice**[10], **Edward T. Eng**[10], **Rick K. Huang**[11], **Rajesh K. Soni**[12], **Brian Kloss**[13], **Zhiheng Yu**[11], **Jonathan A. Javitch**[1,8,9,14], **Wayne A. Hendrickson**[2,9,13], **Paul A. Slesinger**[5], **Matthias Quick**[8,14], **Joseph Graziano**[4], **Hongtao Yu**[15], **Oliver Fiehn**[3], **Oliver B. Clarke**[9,16,*], **Joachim Frank**[2,17,*], **Qing R. Fan**[1,18,*]

[1]Department of Pharmacology, Columbia University, New York, NY, USA.

[2]Department of Biochemistry and Molecular Biophysics, Columbia University, New York, NY, USA.

[3]NIH West Coast Metabolomics Center, University of California Davis, CA, USA.

[4]Department of Environmental Health Sciences, Columbia University, New York, NY, USA.

[5]Nash Family Department of Neuroscience, Friedman Brain Institute, Icahn School of Medicine at Mount Sinai, New York, New York, USA.

[6]Key Laboratory of Receptor Research, Center for Structure and Function of Drug Targets, Shanghai Institute of Materia Medica, Chinese Academy of Sciences, Shanghai, China.

[7]MRC Laboratory of Molecular Biology, Cambridge, UK.

[8]Department of Psychiatry, Columbia University, New York, NY, USA.

[9]Department of Physiology and Cellular Biophysics, Columbia University, New York, NY, USA.

[10]National Resource for Automated Molecular Microscopy, Simons Electron Microscopy Center, New York Structural Biology Center, New York, NY, USA.

[11]Janelia Research Campus, Howard Hughes Medical Institute, Ashburn, VA, USA.

Users may view, print, copy, and download text and data-mine the content in such documents, for the purposes of academic research, subject always to the full Conditions of use:http://www.nature.com/authors/editorial_policies/license.html#terms

[*]**Correspondence and request for materials** should be addressed to oc2188@cumc.columbia.edu (O.B.C.); jf2192@cumc.columbia.edu (J.F.); qf13@cumc.columbia.edu (Q.R.F.).

Author contributions: J.P., J.L., Q.R.F. and K.M.R. cultured cells and purified protein; Z.J.F. and A.F. prepared cryo-EM grids; Z.F., A.F., Q.R.F. and O.B.C. collected cryo-EM data; Z.J.F. and A.F. performed initial image processing; O.B.C. processed cryo-EM data to high resolution; L.M. and Q.R.F. built and refined models; Q.R.F., L.M., A.F., J.P. and Z.F. analyzed structures; T.S. and O.F. identified phospholipids and GABA by mass spectrometry; V.N.S. and J.G. conducted elemental analysis; Q.R.F, J.L., J.P., A.F., J.T., X.L. and J.P.W. performed mutagenesis and cell-based functional assay; M.Q. performed and analyzed radioligand binding studies; B.C, Y.G., H.Z., and Y.K. generated expression plasmids and carried out early protein purification trials; R.G., W.R., E.E., R.K.H., Z.Y. assisted with cryo-EM data collection; S.C., Z.L., W.R. and E.E. performed initial cryo-EM characterization; R.K.S. measured molecular mass; B.K. screened detergents; W.A.H. contributed to structural analysis; Q.R.F., P.A.S. and J.A.J. supervised functional analysis; J.F., O.B.C., and H.Y. supervised cryo-EM studies; Q.R.F. and A.F. wrote the paper; T.S., V.N.S., M.Q., Z.F. and R.K.S. contributed methods sections; all authors contributed to the revision; Q.R.F., A.F., J.P., O.B.C., T.S., Z.F., J.L. and M.Q. prepared figures; Q.R.F. conceived and supervised the project.

Competing interests: The authors declare no competing interests.

Extended data is available for this paper.

Supplementary information is available for this paper.

Author Manuscript Author Manuscript Author Manuscript Author Manuscript

[12]Proteomics Shared Resource, Herbert Irving Comprehensive Cancer Center, Columbia University, New York, NY, USA.

[13]Center on Membrane Protein Production and Analysis, New York Structural Biology Center, New York, NY, USA.

[14]Division of Molecular Therapeutics, New York State Psychiatric Institute, New York, NY, USA.

[15]Howard Hughes Medical Institute, Department of Pharmacology, University of Texas Southwestern Medical Center, Dallas, TX, USA.

[16]Department of Anesthesiology and the Irving Institute for Clinical and Translational Research, Columbia University, New York, NY, USA.

[17]Department of Biological Sciences, Columbia University, New York, NY, USA.

[18]Department of Pathology and Cell Biology, Columbia University, New York, NY, USA.

[19]These authors contributed equally to this work.

Abstract

Human $GABA_B$ G protein-coupled receptor (GPCR), a member of the class C family, mediates inhibitory neurotransmission and is implicated in epilepsy, pain, and addiction[1]. A unique GPCR known to require heterodimerization for function[2–6], its two subunits, $GABA_{B1}$ and $GABA_{B2}$, are structurally homologous but perform distinct and complementary functions. $GABA_{B1}$ recognizes orthosteric ligand[7,8], while $GABA_{B2}$ couples with G protein[9–14]. Each subunit is characterized by an extracellular Venus flytrap (VFT) module, a descending peptide linker, a seven-helix transmembrane (TM) domain, and a cytoplasmic tail[15]. Whereas the VFT heterodimer structure has been resolved[16], the structure of the full-length receptor and its transmembrane signaling mechanism remain unknown. Here we present a near full-length structure of the $GABA_B$ receptor, captured in an inactive state via cryo-electron microscopy (EM). Our structure reveals multiple ligands pre-associated with the receptor, including two large endogenous phospholipids embedded within the TM domains to maintain receptor integrity and modulate receptor function. We also identify a novel heterodimer interface between TM helices 5 and 3 of both subunits, which serves as a signature of the inactive conformation. A unique ′intersubunit latch′ within this TM interface maintains the inactive state, and its disruption leads to constitutive receptor activity.

Architecture of $GABA_B$ receptor

The heterodimeric human $GABA_B$ receptor was assembled using baculovirus-infected mammalian cells. Each subunit was truncated at the carboxyl terminal end according to the domain boundary of the intracellular coiled-coil[17] to eliminate flexible regions (Supplementary Fig. 1). Upon extraction and purification with detergent (Extended Data Fig. 1a,b; Supplementary Fig. 2), the complex bound radioactive [^{3}H]GABA with a dissociation constant comparable to the GABA affinity reported for native receptors[3,4,7] (Extended Data Fig. 1c). Functional analysis incorporating a chimeric $G\alpha_{qi5}$ protein and inositol phosphate (IP) assay[18] in mammalian cells showed that agonist baclofen activated the C-terminally truncated and full-length receptor with similar potency and efficacy, indicating that the

Author Manuscript Author Manuscript Author Manuscript Author Manuscript

deleted regions in the $GABA_{B1b}$ and $GABA_{B2}$ cytoplasmic tails are not required for ligand-mediated G protein activation (Extended Data Fig. 1d).

We determined the structure of the heterodimeric $GABA_B$ receptor by cryo-EM to an overall resolution of 3.3 Å (Extended Data Fig. 2a–e; Supplementary Table 1). The global density map displayed directional anisotropy due to linker flexibility (Extended Data Fig. 2f). Performing local refinement separately on the extracellular (ECD) and TM domains yielded 3.1 Å and 3.4 Å resolution reconstructions, respectively (Extended Data Figs. 2g,h). A composite map combining the ECD and TM reconstructions was used for model building and refinement (Extended Data Fig. 3). By applying three-dimensional variability analysis of the data, we found that the receptor is in dynamic motion, and its functional state corresponds to a continuum of conformations along multiple dimensions (Supplementary Video 1–4).

The heterodimeric $GABA_B$ receptor is assembled by $GABA_{B1b}$ and $GABA_{B2}$ subunits interacting side-by-side while facing opposite directions (Fig. 1a,b; Extended Data Fig. 4). Both the VFT and TM components of the two subunits are related by pseudo two-fold axes. Extracellular and intracellular loops (ECLs and ICLs) that interconnect adjacent helices within each TM are visible in the density map, except for ICL2. The cytoplasmic tail including the coiled-coil domain is disordered, possibly due to its flexible attachment to the TM domain.

The elongated peptide linker joining the VFT to the TM is buttressed through its interaction with a β-hairpin formed by ECL2 (Fig. 1c). ECL2 twists across the linker, forming a united mechanical junction to transmit the conformational changes in the VFT to the TM and vice versa. Additionally, the ECD and TM domains of the receptor spontaneously flex back and forth about the linker, exhibiting the region's intrinsic flexibility (Supplementary Video 1).

Since no ligand was added during protein purification, we expected the receptor to be in an apo form and inactive conformation. To our surprise, we observed multiple ligands bound to the receptor. $GABA_{B1b}$ contains a Ca^{2+} at the interdomain cleft of VFT. In addition, an endogenous phospholipid is bound within the TM pocket of each subunit, with a phosphatidylethanolamine (PE 38:5) in $GABA_{B1b}$, and a phosphatidylcholine (PC 38:2) in $GABA_{B2}$. Finally, ten cholesterol or cholesteryl hemisuccinate molecules, which we modeled as cholesterol (Methods), are distributed around the exterior of the TM complex, including two that interface both subunits.

Inactive conformation of $GABA_B$ receptor

The cryo-EM structure of $GABA_B$ receptor occupies an inactive conformation based on its similarity to the known crystal structures of $GABA_B$ VFT in the apo and antagonist-bound states[16]. First, the VFT module, composed of LB1 and LB2 domains, adopts an open interdomain conformation in both subunits (Extended Data Fig. 5a,b). Second, while an N-terminal LB1-LB1 dimer interface is present in all functional states, the distinct lack of a heterodimer interface between the membrane-proximal LB2 domains is shared by the near full-length cryo-EM structure and inactive-state VFT structures (Extended Data Fig. 5c,d).

Author Manuscript Author Manuscript Author Manuscript Author Manuscript

In contrast, a hallmark of the active-state VFT structures is a novel heterodimer interface between LB2 domains, which results from agonist-induced $GABA_{B1b}$ closure[16].

Using conformational variability analysis, we observed that the LB2 domains of both subunits fluctuate by approaching and withdrawing from the central vertical axis of the heterodimer, yet never make contact as in active-state VFT crystal structures (Supplementary Video 2,3). The motion exhibited by the LB2 domains and their associated linkers suggests that the inactive functional state corresponds to an ensemble of conformations, where the separation between the membrane proximal regions falls within a small range around the coordinates of the current structure.

TM heterodimer interface in the inactive state

We identified a novel heterodimer interface between the TM5 and TM3 helices of both subunits, that embodies the signature of the $GABA_B$ inactive conformation (Fig. 2a). A TM5-TM5 contact has previously been detected through crosslinking of the $GABA_B$ receptor[19], but TM dimer interfaces of any kind are yet to be found in other inactive class C GPCRs, including the recent inactive metabotropic glutamate receptor $mGlu_5$ structure[20] (Extended Data Fig. 5e).

Positioned at 30° from the extracellular dimer interface, the TM dimer interactions bury approximately 740 $Å^2$ of surface area and exhibit high shape complementarity (Extended Data Fig. 5f). The pair of TM5 helices scissor at their central residues before contacting the transverse TM3 of opposing subunits at their intracellular ends (Fig. 2a). TM5 extracellular ends display conformational variance wherein they approach and withdraw but fail to make contact (Supplementary Video 4). All direct heterodimer interactions occur near the cytoplasmic membrane surface and can be divided into three core layers (I-III) along the helical path of TM5 (Fig. 2a).

The surface layer I caps the extracellular end of the TM heterodimer interface. It is comprised of hydrophobic contacts between four leucine residues of both subunits. The middle layer II lies directly beneath layer I, and consists of three phenylalanine residues packing against one another, as well as their neighboring leucine residues. Both layers solely incorporate TM5 residues.

Layer III, consisting of sections IIIa and IIIb, completes the interface at the intracellular end. IIIa possesses a network of salt-bridges that tether the cytoplasmic ends of $GABA_{B1b}$ and $GABA_{B2}$ TM domains. This critical interaction is mediated by a quartet of charged residues from TM3 and TM5 helices ($GABA_{B1b}$: $His572^{3.55}$ and $Glu673^{5.60}$; $GABA_{B2}$: $His579^{3.55}$ and $Glu677^{5.60}$) (Supplementary Table 2), a feature we refer to as the ′intersubunit latch′ for securing the TM orientation of the two subunits in the inactive conformation. One of the ′intersubunit latch′ residues shares nonpolar contacts with a lysine of $GABA_{B2}$ TM5, establishing the accessory site IIIb.

In addition, the central layers of direct heterodimer contacts are flanked on each side by a cholesterol molecule. One mediates the interaction between TM5 helices of both subunits

Author Manuscript Author Manuscript Author Manuscript Author Manuscript

(CLR3), while the other bridges TM3 of $GABA_{B1b}$ and TM5 of $GABA_{B2}$ (CLR6) (Extended Data Fig. 5g).

The ′intersubunit latch′

To determine the importance of the ′intersubunit latch′ in controlling the inactive state of $GABA_B$ receptor, we examined the effect of single charge-repelling mutations ($GABA_{B1b}$-E673R; $GABA_{B2}$-H579E) within the motif. Wild-type $GABA_B$ receptor exhibited basal activity in the absence of agonist (Fig. 2b), as previously reported[14]. Both mutants substantially increased basal activity when compared to wild-type, suggesting that each mutation promotes agonist-independent constitutive activity (Fig. 2b). The basal activity displayed by these mutants reached approximately 80–90% of the maximal agonist-dependent wild-type response (Fig. 2b,c). Application of the agonist baclofen raised receptor activity further to the highest wild-type level (Fig. 2c). Neither mutation altered the agonist potency. After treating each construct with the inverse agonist CGP54626, the basal activity of mutants still remained higher than that of wild-type, providing further evidence that the ′intersubunit latch′ mutations serve to shift the conformational equilibrium of $GABA_B$ receptor towards an active state. Taken together, our mutational data indicate that the ′intersubunit latch′ is fundamental to maintaining the inactive state of the receptor.

Endogenous ligands bound to $GABA_{B1b}$ VFT

We identified a novel potential Ca^{2+}-binding site in the vicinity of the orthosteric ligand-binding cleft on the LB2 surface of $GABA_{B1b}$ (Fig. 3a; Extended Data Fig. 6a,b). The metal ion density has remarkable peak height in the cryo-EM density map (10σ) and is surrounded by residues chemically favorable for Ca^{2+} coordination. The Ca^{2+} is anchored by the carboxylate groups of three acidic residues (Asp281, Glu309, and Glu423) as well as the backbone carbonyl atoms of two additional residues (Gly277 and Tyr279) (Fig. 3b). The Ca^{2+}-oxygen bond distances are between 3.0 Å and 4.6 Å, suggesting that the ion is in a hydrated state. The Ca^{2+} location in $GABA_{B1b}$ is different from any of the multiple sites found in calcium-sensing (CaS) receptor[21], another class C GPCR (Fig. 3c).

Using inductively coupled plasma mass spectroscopy, we detected the presence of Ca and Cu above background level in purified $GABA_B$ receptor. The amounts of other metal elements were negligible (Supplementary Table 3). The molar ratios of Ca and Cu relative to the receptor protein (0.43:1 and 0.51:1) suggest partial occupancy of the ion-binding sites. An unmodeled density within the interdomain cleft, coordinated by tryptophan and histidine, may serve as a potential Cu^{2+}-binding site but lacks sufficient signal to be labeled confidently.

In exploring the functional role of the bound ion, we found that the Ca^{2+} chelator EGTA substantially reduced $GABA_B$ receptor basal activity, and that mutating specific coordinating residues ($GABA_{B1b}$-E309K and $GABA_{B1b}$-E423R) had similar, although less drastic, effects (Extended Data Fig. 6c,d). Consistent with previous findings, these data suggest that Ca^{2+} may act as a positive allosteric modulator of $GABA_B$ receptor[22,23]. Our structure implies

Author Manuscript Author Manuscript Author Manuscript Author Manuscript

that Ca^{2+} stabilizes residues adjacent to the critical agonist-binding residue Trp278, thereby indirectly reinforcing its conformation (Fig. 3b).

We also found density in the orthosteric agonist-binding site of $GABA_{B1b}$, and its shape suggests a GABA-like endogenous ligand (Extended Data Fig. 6a,b). GABA is a potential candidate since it fits the density and was detected in the lysate of cells used to express the receptor (Extended Data Fig. 6e,f). This GABA-like endogenous ligand bound in an inactive receptor conformation may reflect a pre-activation state; however, further investigation is required.

Discovery of endogenous phospholipid ligands

Our structure revealed endogenous phospholipids within the TM domains of both $GABA_B$ subunits. Using CaS receptor as control in mass spectrometry, we identified two phospholipids specifically bound to $GABA_B$ receptor, PE 38:5 and PC 38:2 (Fig. 4a–d). Both lipids consist of two long-chain fatty acyl moieties of 18 and 20 carbons. We further assigned PE 38:5 to $GABA_{B1b}$ and PC 38:2 to $GABA_{B2}$ based on the size difference between phosphoethanolamine and phosphocholine head groups of the two lipids (Extended Data Fig. 7a,b). The lipid density in the $GABA_{B2}$ TM domain has a bulkier head group that can better accommodate the larger choline moiety of PC 38:2.

Mirroring the amphipathicity of phospholipids, the lipid-binding pocket of each $GABA_B$ subunit retains a hydrophilic trunk and two lipophilic branches for binding the lipid polar head and nonpolar tails, respectively. The trunk consists of a negatively charged patch covering the amine moiety, and a positively charged area surrounding the phosphate (Extended Fig. 7c,d). The lipid-binding pockets are notably deep, extending from the extracellular membrane surface to the center of the TM domain (Fig. 4e,f). Each lipid occupies nearly the entire range of ligand-binding positions in class A, B, C and F GPCRs (Extended Data Fig. 7e–h).

Each $GABA_B$ subunit makes extensive contacts with the bound lipid, utilizing a majority of the TM helices, including TM2, 3, 5, 6, and 7 (Extended Data Fig. 7i,j). Approximately 2,400 $Å^2$ of surface area is buried by either lipid-subunit pair. In addition, ECL2 directly contacts PE 38:5 in $GABA_{B1b}$, while the linker and all three ECLs interact with PC 38:2 in $GABA_{B2}$.

Key elements of the lipid-receptor interactions are conserved in $GABA_{B1b}$ and $GABA_{B2}$ (Fig. 4g–j; Extended Data Figs. 7i,j; Supplementary Fig. 3). First, the hydrophilic head of each lipid is anchored through interactions with conserved histidine and arginine residues ($GABA_{B1b}$: His643 of ECL2 and $Arg549^{3.32}$; $GABA_{B2}$: His647 of ECL2 and $Arg556^{3.32}$) (Fig. 4g,h). $GABA_{B2}$ also incorporates Arg714 of ECL3, rendering the lipid-binding pocket more electropositive than that of $GABA_{B1b}$ (Fig. 4h).

Second, the 20-carbon fatty acyl chain of both lipids follows a perpendicular turn to pass between two aromatic residues ($GABA_{B1b}$: $Phe557^{3.40}$ and $Tyr657^{5.44}$; $GABA_{B2}$: $Tyr564^{3.40}$ and $Tyr661^{5.44}$) (Fig. 4i,j). A cis double bond in each fatty acyl chain forms **π** interactions with the aromatic side chains. The bend is further buttressed by extensive

Author Manuscript Author Manuscript Author Manuscript Author Manuscript

nonpolar contacts with the aliphatic part of a conserved lysine ($GABA_{B1b}$-Lys660$^{5.47}$; $GABA_{B2}$-Lys664$^{5.47}$) lying parallel to the chain. Finally, the 18-carbon fatty acyl chain of both lipids is relatively straight, extending toward the cytoplasm in a binding pocket lined by small aliphatic residues on TM2, 3, and 7 (Fig. 4i,j).

The $GABA_B$ receptor TM domains are covered by the linker and ECLs, which form a lid over the lipid-biding pocket. Phospholipids may access the lipid-binding pocket of designated subunits laterally through gaps between TM5 and 6 (Extended Data Fig. 8a–d). One of the fatty acyl tails of each phospholipid even protrudes through this opening. The lipid-binding sphingosine 1-phosphate ($S1P_1$) receptor possess a similar gap between TM1 and TM7[24] (Extended Data Fig. 8e,f). The endogenous lipids of other GPCRs can be readily replaced[24], but the size and engagement of the endogenous lipids bound to $GABA_B$ receptor suggest that they are critical for maintaining receptor integrity and stability.

To explore the physiological relevance of the endogenous phospholipids, we mutated residues that hydrogen bonded with the phosphate head group. We identified R714A in $GABA_{B2}$ ECL3, which displayed a small gain of function despite reduced cell surface expression (Extended Data Fig. 8g,h). This mutation is expected to enhance the movement of PC 38:2 within $GABA_{B2}$ by eliminating a critical interaction with the lid. Our results suggest that PC 38:2 may act as a negative allosteric modulator of $GABA_B$ receptor by stabilizing the inactive conformation of $GABA_{B2}$.

Comparison of individual subunits with other GPCRs

The $GABA_{B1b}$ and $GABA_{B2}$ subunits have highly similar VFT and TM components but differ in their relative orientation (Extended Data Fig. 9a,b). Each subunit differs from all other class C GPCRs in possessing an extended peptide linker between the VFT and TM domain instead of a cysteine-rich domain. (Fig. 1c).

$GABA_B$ subunits also display distinct helix positions in the seven-helix bundles among inactive GPCRs (Extended Data Fig. 9c–f). However, these differences are minor compared to the dramatic movement of TM6 in class A and B GPCRs when activated upon G protein coupling[25,26]. This corroborates our conclusion that we have captured an inactive conformation of the $GABA_B$ receptor.

$GABA_B$ receptor presents unique variations of conserved TM motifs (Extended Data Fig. 10a,b). In most class A GPCRs such as rhodopsin[27], the ′ionic lock′ tethers TM3 and TM6 to stabilize the inactive state of an individual TM domain[27] (Extended Data Fig. 10c). The ′ionic locks′ of both $GABA_B$ subunits consist of an aspartate from ICL3 and a lysine in TM3 (3.50) (Extended Data Fig. 10a,b). Although only the Lys/Asp pair in $GABA_{B1b}$ are within hydrogen bond distance, their backbone Cα-Cα separations (9.3–9.4 Å) are comparable to that of rhodopsin[27] (8.7 Å) and inactive mGlu receptors[28,29] (10.9–11.2 Å), indicating that the ′ionic lock′ is intact within both $GABA_B$ subunits (Extended Data Fig. 10a–e).

The ′ionic lock′ in each $GABA_B$ subunit resides in close proximity to an FxPKxx sequence in TM7, which is the counterpart of the NPxxY$(x)_{5,6}$F motif in class A GPCRs[25].

Author Manuscript Author Manuscript Author Manuscript Author Manuscript

Specifically, the conserved Lys$^{7.51}$ participates in a network of hydrophilic contacts with the ′ionic lock′ through Asn$^{2.39}$ and a serine in ICL1 (Extended Data Fig. 10a, b; Supplementary Fig. 3). These interactions unite the ′ionic lock′ and FxPKxx motif into a larger and integral system for maintaining the inactive TM conformation of individual $GABA_B$ subunits.

Conclusion

The combination of our previous VFT structures and current cryo-EM data supports the occurrence of three critical events during $GABA_B$ receptor activation: (1) agonist-induced VFT closure of $GABA_{B1b}$, (2) association of membrane-proximal LB2 domains, and (3) dissociation of the ′intersubunit latch′ and the ensuing rearrangement of the TM heterodimer interface. This hypothesis is consistent with our finding that an inverse agonist bound to the extracellular domain can inhibit the constitutive activity stemming from the spontaneous closure of $GABA_{B1b}$ VFT, but not that resulting from direct ‘downstream’ disruption of the ′intersubunit latch′.

The $GABA_B$ receptor structure also yields surprising findings regarding its endogenous ligand composition. We suspect that the phospholipids discovered well inside each TM cavity are necessary structural components, as they are pre-bound within each subunit and their interactions with the receptor are extensive. These endogenous lipids may be unique to $GABA_B$ receptor since the lipid-binding residues are not conserved among class C GPCRs (Supplementary Fig. 3). Pre-occupation of the TM pocket suggests that $GABA_B$ allosteric modulators may bind to yet unknown sites, with the heterodimer interface being a potential location. An active structure of $GABA_B$ receptor would confirm whether the phospholipids are integral receptor components or functional modifiers.

Methods

Protein expression and purification

Human $GABA_{B1b}$ (UniProt code: Q9UBS5–2) and $GABA_{B2}$ (UniProt code: O75899) subunits were each cloned into a modified pEG BacMam vector[30] for co-expression in baculovirus-infected mammalian cells. $GABA_{B1a}$ and $GABA_{B1b}$ are two major isoforms of $GABA_{B1}$, and have identical pharmacological profiles[7]. Different C-terminal truncations of each receptor subunit were tested for heterodimeric receptor assembly. The optimal $GABA_{B1b}$ expression construct consisted of residues 1–802 [$GABA_{B1b}$(1–802)], while $GABA_{B2}$ construct included residues 1–819 [$GABA_{B2}$(1–819)]. This allowed the heterodimeric construct to transport to the cell membrane as it retained the intracellular coiled-coil region present in the intracellular tails of each subunit[31,32]. Signal peptides for $GABA_{B1b}$ and $GABA_{B2}$ occupied residues 1–29 and 1–41, respectively. A Flag tag was engineered at the C terminus of each subunit to facilitate affinity purification.

Human embryonic kidney (HEK) 293 GnTI$^-$ cells[33] were grown in suspension culture at 37°C in 8% CO_2 using 293 freestyle media (Life Technology, Carlsbad, USA). The cells were co-infected with recombinant baculoviruses carrying the $GABA_{B1b}$(1–802) and $GABA_{B2}$(1–819) genes at 37°C. To enhance expression level, 10 mM sodium butyrate was

Author Manuscript Author Manuscript Author Manuscript Author Manuscript

added 18 hours post infection, and the cells were incubated for an additional 72 hours at 30°C before harvest.

Cell membrane was isolated by differential centrifugation method. The cells were lysed using an EmulsiFlex-C3 high pressure homogenizer (Avestin, Ottawa, Canada) in a buffer containing 50 mM HEPES, pH 7.5, 150 mM NaCl, 10% glycerol and a cocktail of protease inhibitors (Roche, Basel, Switzerland). Cell debris was removed by centrifugation of the lysed cell suspension at 10,000 rpm. The cell membrane was then pelleted by ultracentrifugation at 45,000 rpm.

$GABA_B$ receptor was extracted from the cell membrane with 50 mM HEPES, pH 7.5, 150 mM NaCl, 10% glycerol, 1% lauryl maltose neopentyl glycol (LMNG) (Anatrace, Maumee, USA), and 0.2% cholesteryl hemisuccinate (CHS) (MilliporeSigma, Burlington, USA) at 4°C overnight. After the insoluble matter was removed by centrifugation, the supernatant was applied to an anti-Flag M2 antibody affinity column. The column was washed stepwise with decreasing concentrations of detergent, from 0.1% to 0.002% LMNG. The heterodimeric $GABA_{B1b}$(1–802)-$GABA_{B2}$(1–819) complex was then eluted with 50 mM HEPES, pH 7.5, 50 mM NaCl, 0.002% LMNG, 0.0004% CHS, and 0.2 mg/ml Flag peptide.

The receptor was further purified by Mono Q (GE Healthcare, Chicago, USA) ion exchange chromatography using a linear salt gradient from 50 mM to 1 M NaCl in 50 mM HEPES, pH 7.5, 0.002% LMNG, and 0.0004% CHS. Finally, the assembled $GABA_B$ receptor was subjected to Superose 6 (GE Healthcare, Chicago, USA) size exclusion chromatography in 50 mM HEPES, pH 7.5, 50 mM NaCl, 0.002% LMNG, and 0.0004% CHS.

HEK 293 GnTI$^-$ cells were purchased from and authenticated by American Type Culture Collection (ATCC No. CRL-3022). Cell morphology was examined for each passage of cells. The cells were certified by ATCC to be free of mycoplasma contamination, but they were not tested again during culturing.

Cryo-EM specimen preparation and data acquisition

Specimens were composed of vitrified $GABA_B$ protein samples occupying UltraAuFoil R 0.6/1, 300 mesh holey Au/Au grids (Quantifoil Micro Tools, Jena, DEU). The surfaces of the grids were rendered hydrophilic by glow-discharging using H_2 and O_2 for 25 seconds at 10 watts with a Solarus 950 plasma cleaner system (Gatan, Cranberry, USA). For vitrification, 3ul of purified $GABA_B$ receptor at a concentration of approximately 0.3 mg/ml was applied to each grid, blotted for 4 seconds at a blot force of 3 inside a Vitrobot Mark IV (Thermo Fisher Scientific, Waltham, USA), and plunge-frozen in a liquid propane:ethane mixture (63:37, v/v) cooled with liquid nitrogen.

Data collection was performed on a Titan Krios transmission electron microscope (Thermo Fisher Scientific, Waltham, USA) equipped with a K2 Summit direct electron detection camera (Gatan, Cranberry, USA) in counting mode and a post-column GIF Quantum energy filter (Gatan, Cranberry, USA) in zero-energy-loss mode with a slit width of 20 eV. Micrographs were accrued at a calibrated pixel size of 1.06 Å and with nominal defocus range of −0.5 to −2 μm. Each micrograph consisted of 60 frames collected over a 12-second

Author Manuscript Author Manuscript Author Manuscript Author Manuscript

exposure at a dose rate of ~8 e^{-}/pixel/second for a total dose of ~85 $e^{-}/Å^2$. A total of 3,435 micrographs were acquired as dose-fractionated image stacks.

Cryo-EM image processing

Image processing began with frame alignment and dose-weighting of the image stacks using the CPU-based implementation of MotionCor2[34] in Relion 3.0[35]. Estimation of contrast transfer function (CTF) for each non-dose weighted micrograph was determined by Gctf[36] v1.06. After visual inspection of the micrographs and their power spectra, 3,334 were selected for further processing.

Approximately 3,000 particles were manually picked in Relion 3.0[35], and extracted from a 4x binned dataset with a pixel size of 4.24 Å. This data produced an initial set of two-dimensional (2D) classes that were used as templates to select 1,048,241 particles automatically, all of which were subsequently imported into cryoSPARC v2[37] for extensive 2D classification. After elimination of unfit classes, a total of 312,840 particles from the high-quality 2D classes were combined to produce an *ab initio* 3D reference in cryoSPARC v2[37]. Based on the *ab initio* model, particles were re-extracted at full scale from the unbinned dataset with a pixel size of 1.06 Å in Relion 3.0[35], and re-introduced into cryoSPARC v2[37] for 3D refinement. Homogeneous refinement of the *ab initio* 3D model against the unbinned set of particles yielded a density map with nominal resolution of 3.6 Å according to the Fourier shell correlation (FSC) = 0.143 gold standard criterion[38]. Heterogenous refinement of multiple models obtained before and after homogeneous refinement allowed removal of additional poor-quality particles and reduced the particle count to 233,737. Non-uniform refinement then improved the resolution to 3.5 Å. At this point, CTF refinement and Bayesian polishing were conducted in Relion 3.0[35], followed by an additional round of non-uniform refinement in cryoSPARC v2[37], further improving the resolution to 3.3 Å.

Although the TM domains of $GABA_B$ receptor exhibit pseudo two-fold symmetry, bulky carbohydrate densities that are visible only in the ECD of $GABA_{B1b}$ subunit resulted in sufficient low-resolution asymmetry to prevent particle misalignment. These include partial carbohydrate densities attached to Asn323 and Asn365 of $GABA_{B1b}$ that do not have counterparts in $GABA_{B2}$.

The global density map exhibited directional anisotropy[39] that is caused by inter-domain movement about a flexible linker. To eliminate the adverse effect of such movement on map quality, we performed local refinement of the ECD and TM domains of $GABA_B$ receptor independently. A mask was created covering each region, and the non-uniform refinement algorithm was used as implemented in cryoSPARC v2[37]. The resulting reconstructions for the individual ECD and TM domains reached 3.1 Å and 3.4 Å resolution, respectively. A composite map was generated in UCSF Chimera[40] by taking the maximum values pointwise from the two locally refined maps after alignment to the global reconstruction (*vop maximum* command in UCSF Chimera[40]). This composite map was used for subsequent model building and refinement.

Author Manuscript Author Manuscript Author Manuscript Author Manuscript

Resolutions of cryo-EM reconstructions were determined using a cutoff value of 0.143 in gold standard half-map Fourier shell correlation (FSC) curves[38].

Three-dimensional (3D) variability analysis[41] was conducted in cryoSPARC v2[37] using the 233,737 particles from global non-uniform refinement as input. Calculations were performed for the entire receptor, the ECDs, and the TM domains, respectively. In each case, multiple modes of variability were solved, and represented as eigenvectors along which conformational changes occur. To visualize the transformation of density, five reconstructions were calculated along each eigenvector, with a filter resolution of 4.5 Å. A movie that combines these reconstructions as frames was generated in Chimera[40] for each dimension of motion.

Model building and refinement

Model building was carried out in COOT[42]. The crystal structure of human $GABA_{B1b}$ VFT-$GABA_{B2}$ VFT complex in the apo form (PDB code: 4MQE) was used as the initial model for extracellular domain of the receptor. The VFT modules of $GABA_{B1b}$ and $GABA_{B2}$ were separately placed into density as rigid bodies. Individual residues were then adjusted to optimize the fit. The linker and TM domain of each subunit was traced *de novo* based on the density. The final model contained residues 48–368, 377–576 and 588–747 of $GABA_{B1b}$, and 54–294, 302–376, 385–584, and 595–749 of $GABA_{B2}$.

In addition to the polypeptide chains, we built models for a Ca^{2+} in the extracellular domain of $GABA_{B1b}$, as well as one phospholipid (PE 38:5 in $GABA_{B1b}$; PC 38:2 in $GABA_{B2}$) within the TM domain of each subunit. Density for carbohydrate was observed at three N-linked glycosylation sites on $GABA_{B1b}$ (Asn365, Asn385 and Asn397), and one site on $GABA_{B2}$ (Asn404). An N-glucosamine residue was modeled at each of these glycosylation sites. Continuous density was also identified for ten cholesterol or CHS molecules surrounding the TM domains of both $GABA_B$ subunits. Cholesterols were modelled to optimize the fit with density, however, these densities may belong to CHS molecules with disordered parts. Density for an endogenous ligand was found at the interdomain cleft of $GABA_{B1b}$ VFT. Although this density could be fit with GABA, it was not modelled because the origin and identity of the ligand remained ambiguous without confirmation by an independent method.

The entire structure was refined by the real-space refinement algorithm, and validated with the comprehensive validation application as implemented in Phenix[43]. Ramachandran statistics was calculated using MolProbity[44]. The refined model also has an overall EMRinger[45] score of 2.7, while the extracellular and TM domains have scores of 3.4 and 1.8, respectively. The final model revealed that VFT and TM components are related to their counterparts in the other subunit by 177° and 179°-rotations about the vertical axis, respectively.

Pairwise structural alignment was performed using LSQMAN[46]. Figures were generated using Pymol Molecular Graphics System Version 2.3 (Schrödinger), UCSF Chimera[40] and UCSF ChimeraX[47]. Software installation support was provided by SBGrid[48].

Author Manuscript Author Manuscript Author Manuscript Author Manuscript

Scintillation proximity assay

Binding of [^{3}H]GABA (60 Ci/mmol; American Radiolabeled Chemicals, Inc., St. Louis, USA) to $GABA_B$ receptor was measured with the scintillation proximity assay (SPA)[49,50]. Purified $GABA_{B1b}$(1–802)-$GABA_{B2}$(1–819) complex (100 ng) was extensively dialyzed against the purification buffer to remove any residual endogenous ligand. The dialyzed protein was then immobilized to yttrium silicate (YSi) protein A SPA beads (62.5 μg) (PerkinElmer, Waltham, USA) using anti-Flag M2 antibody (12.5 pg) (Sigma-Aldrich, Inc., St. Louis, USA), and incubated at 4°C for 30 minutes in the same buffer as used for the final step of protein purification (50 mM Hepes, pH 7.5, 50 mM NaCl, 0.002% LMNG, 0.004% CHS). Increasing concentrations (ranging from 0.2–25 μM) of [^{3}H]GABA (2.5 Ci/mmol final specific radioactivity) were added to the protein/antibody/SPA-bead mixture and the samples were allowed to reach equilibrium at 4°C for 16 hours. Reaction performed with an antibody/SPA-bead mixture in the absence of $GABA_B$ receptor was used to determine the non-proximity signal originating from non-specific interaction between the radioligand and SPA beads.

All samples were counted in a Microbeta™ counter (PerkinElmer, Waltham, USA) in counts per minute (cpm) in the SPA mode. The efficiency of detection was calculated with a standard curve of known [^{3}H]GABA concentrations, and this was used to transform cpm into pmol. Specific binding was determined by subtracting the non-proximity signal (non-specific binding) from the total binding signal and was plotted as a function of free radioligand concentration. Nonlinear regression fitting of the data was performed in SigmaPlot 13.0 to obtain the dissociation constant (K_d) and the molar ratio of GABA-to-receptor binding.

Identification of phospholipid ligands and GABA

Identification of bound endogenous lipids was conducted utilizing published protocol[51] with modifications. Briefly, intact $GABA_B$ and control CaS receptor were digested with trypsin overnight at 37°C. Digested proteins were dried and extracted with 1 mL of ice-cold methanol:water (9:1, v/v). The supernatants were dried and re-suspended with methanol:toluene (9:1, v/v) to equivalent concentration of 2 μM. For LC-MS/MS analysis[52], the lipid extracts were separated on a Waters Acquity UPLC CSH C18 column (100 × 2.1 mm; 1.7 μm) coupled to an Acquity UPLC CSH C18 VanGuard precolumn (5 × 2.1 mm; 1.7 μm). The column was maintained at 65°C at a flow rate of 0.6 mL/min. The mobile phases consisted of A: acetonitrile:water (60:40, v/v) with ammonium formate (10 mM) and formic acid (0.1%), as well as B: 2-propanol:acetonitrile (90:10, v/v) with ammonium formate (10 mM) and formic acid (0.1%). The 15 min separation was conducted under the following gradient: 0 min 15% B; 0–2 min 30% B; 2–2.5 min 48% B; 2.5–11 min 82% B; 11–12 min 99% B; 12–15 min 15% B. Q Exactive HF mass spectrometer (Thermo Fisher Scientific, Waltham, USA) was operated in electrospray ionization (ESI) in positive mode with the following parameters: mass range 100–1500 m/z; spray voltage +3.6 kV; sheath gas (nitrogen) flow rate 60 units; auxiliary gas (nitrogen) flow rate 25 units, capillary temperature 320°C, full scan MS1 mass resolving power 60,000, data-dependent MS/MS acquisition (dd-MS/MS) 4 scans per cycle, dd-MS/MS mass resolving power 15,000. The mass features that were differentially higher in $GABA_B$ receptor were subjected to targeted

Author Manuscript Author Manuscript Author Manuscript Author Manuscript

MS/MS in re-injections to acquire tandem mass spectra. Thermo Xcalibur 4.0.27.19 was used for data acquisition. Data processing and identification were performed in MS-DIAL v3.40. Identification was conducted by matching accurate mass, tandem mass spectra, and chromatographic retention time with built-in lipid library LipidBlast[53]. The identified endogenous lipids bound to $GABA_B$ receptor include phosphatidylcholine (PC) 38:2 [PC(18:1_20:1); International Chemical Identifier (InChI) Key: QLEJPADMSQQACL-WWUFLCHTSA-N], and phosphatidylethanolamine (PE) 38:5 [PE(18:1_20:4); InChIKey: VFUVYNGTMNUBMF-ZRVIQYDLSA-N]. Although many isoforms exist for these lipids, both phospholipids share two long-chain fatty acyl moieties of 18 and 20 carbons based on mass spectrometry fragmentation pattern and biological relevance.

Identification of GABA was conducted in targeted LC-MS/MS. Briefly, cell supernatant, cell lysate, together with culture media and lysis buffer controls were dried from 1 mL and extracted with 1 mL of ice-cold methanol:water (9:1, v/v). The supernatants were dried and re-suspended with 200 μL of acetonitrile:water (8:2, v/v). The extracts were separated on a Waters Acquity UPLC BEH Amide column (150 × 2.1 mm; 1.7 μm) coupled with an Acquity UPLC BEH Amide VanGuard precolumn (5 × 2.1 mm; 1.7 μm). The column was maintained at 45 °C at a flow rate of 0.4 mL/min. Mobile phase A was water with ammonium formate (10 mM) and formic acid (0.125%) while B was acetonitrile:water (95:5, v/v) with ammonium formate (10 mM) and formic acid (0.125%). Separation was conducted using the gradient: 0–2 min 100% B; 2–7.7 min 70%B; 7.7–9.5 min 40% B; 9.5–12.5 min 30% B; 10.25–12.75 100% B, 12.75–16.75 100% B. Q Exactive HF mass spectrometer was operated in the same parameters as above. GABA standard was injected along with the samples to confirm its spectrum and retention time. The responses of GABA in samples were normalized to that of GABA standard with known concentration.

Cell surface expression

Full-length human $GABA_{B1b}$ and $GABA_{B2}$ were each cloned into a pcDNA3.1(+) vector (Life Technologies, Carlsbad, USA), with a Flag tag inserted after the signal peptide of $GABA_{B1b}$, and an HA tag after the signal peptide of $GABA_{B2}$. Similar constructs were also generated for the C-terminally truncated $GABA_{B1b}$(1–802) and $GABA_{B2}$(1–819). Single mutants of full-length $GABA_{B1b}$ (E673R, E309K, and E423R) and $GABA_{B2}$ (H579E, R714A) were constructed using the QuikChange mutagenesis system (Agilent Technologies, Santa Clara, USA).

The cell surface expression levels of wild-type (WT) and mutant $GABA_B$ receptor were measured following previously published protocol[17]. Briefly, HEK293 T/17 cells (ATCC) were cultured in monolayer in DMEM/F12 media (Life Technology, Carlsbad, USA) supplemented with 10% FBS at 37°C in the presence of 5% CO_2. The cells were co-transfected with $GABA_{B1b}$ and $GABA_{B2}$ plasmids using Lipofectamine 3000 (Life Technologies, Carlsbad, USA). Each $GABA_{B1b}$ and $GABA_{B2}$ mutant was paired with its wild-type partner. Since $GABA_{B1b}$ is retained inside the cells unless it is chaperoned by $GABA_{B2}$, we used the surface expression level of $GABA_{B1b}$ on intact cells to measure the amount of assembled heterodimeric $GABA_B$ receptor on the cell surface. The amount of surface $GABA_{B1b}$ protein detected for each pair of constructs was normalized with the cell

Author Manuscript Author Manuscript Author Manuscript Author Manuscript

count in each experiment. The cell surface expression level of each mutant is calculated as a percentage of the wild-type receptor.

After blocking with 1% BSA, the cells were incubated with mouse anti-Flag M1 antibody (MilliporeSigma, Burlington, USA) as the primary antibody to measure $GABA_{B1b}$ expression, followed by donkey anti-mouse IRDye 800-labeled antibody (Li-Cor Biosciences, Lincoln, USA) as the secondary antibody. Fluorescent signals were measured with an Odyssey Infrared Imager (Li-Cor Biosciences, Lincoln, USA). Each experiment was performed in triplicates.

HEK 293 T/17 cells were purchased from and authenticated by American Type Culture Collection (ATCC No. CRL-11268). Cell morphology was examined for each passage of cells. The cells were certified by ATCC to be free of mycoplasma contamination, but they were not tested again during culturing.

Inositol phosphate measurement

HEK293 T/17 cells were co-transfected with plasmids encoding $GABA_{B1b}$, $GABA_{B2}$, and $G\alpha_{qi5}$. The $G\alpha_{qi5}$ chimera was constructed by replacing the five C-terminal amino acids of murine $G\alpha_q$ with those of murine $G\alpha_i$[18]. Exchanging the C-terminal end of $G\alpha_q$ with that of $G_{i/o}$ permits it to couple with $GABA_B$ receptor and allows the functional activity of the receptor to be tracked through phospholipase C (PLC). Control experiments were conducted using cells transfected with an empty pcDNA3.1(+) vector, $G\alpha_{qi5}$ alone, or wild-type $GABA_{B1b}$ and $GABA_{B2}$ in the absence of $G\alpha_{qi5}$.

Inositol phosphate (IP) accumulation was quantified with the homogenous time-resolved fluorescence (HTRF) IP-one Tb kit (Cisbio Bioassays, Codolet, FRA), which measures the accumulation of inositol 1-monophosphate (IP_1), a metabolite of inositol 1,4,5-triphosphate (IP_3). One day post transfection, the cells were stimulated with increasing concentrations of baclofen for one hour at 37°C. The stimulated cells were lysed, and the native IP_1 which had been produced was incubated with a d2 fluorophore-labeled IP_1 analog (acceptor) to compete for binding to an Eu Cryptate-coupled anti-IP1 monoclonal antibody (donor). The fluorescence data was collected at 620 and 665 nm with a PHERAstar FS plate reader (BMG LABTECH, Cary, USA) after laser excitation at 320 nm. The fluorescence resonance energy transfer (FRET) signal was calculated as the fluorescence ratio (665 nm/620 nm) and is inversely proportional to the concentration of native IP_1 produced following $GABA_B$ activation through a chimeric $G\alpha_{qi5}$ G protein. The agonist-induced receptor response of each mutant was calculated as a percentage of the maximum activity of wild-type receptor relative to the activity observed for $G\alpha_{qi5}$ alone. Basal activity was determined in the absence of baclofen stimulation and calculated similarly as the agonist-dependent receptor response. Data analysis was performed using the non-linear regression algorithms in Prism (GraphPad Software, San Diego, USA). Data points represent average ± s.e.m. of multiple experiments, each consisting of quadruplicate measurements.

Application of a known antagonist, CGP54626, reduced agonist potency as expected. In addition, the compound lowered the basal activity of $GABA_B$ receptor, indicating that it has

Author Manuscript Author Manuscript Author Manuscript Author Manuscript

inverse agonist activity as previously reported[54]. Therefore, we refer to the compound as an inverse agonist.

Inductively coupled plasma mass spectrometry

Purified $GABA_B$ receptor (200 µl, 11.1 µg/µL or 57.7 µM) was collected in metal-free tubes and digested overnight with the addition of 1 mL of concentrated nitric acid ($HNO_{3)}$ (Fisher, Hampton, USA; Optima grade). The digested protein was then diluted to a total volume of 10 ml with 8.7 ml of deionized water supplemented with 500 µg/L of gold (Au) and 100 µL of an internal standard solution containing 500 µg/L each of gallium (Ga) and rhodium (Rh) in 2% HNO3. The protein purification buffer (200 µl) containing 10 mM HEPES, pH 7.5, 50 mM NaCl, 0.002% LMNG, and 0.0004% CHS, was similarly mock digested and diluted for analysis.

Inductively coupled plasma mass spectrometry (ICP-MS) was conducted using a NexION 350S ICP-MS instrument (Perkin Elmer, Waltham, USA) equipped with dynamic reaction cell (DRC) feature and a SC-4 DX FAST Autosampler (Elemental Scientific, Omaha, USA). The DRC-ICP-MS experimental method was developed based on previously published procedures[55,56] and a laboratory protocol for multi-element DCR-ICP-MS from the Centers for Disease Control (CDC) (https://www.cdc.gov/nchs/data/nhanes/nhanes_13_14/UM_UMS_UTAS_UTASS_H_MET.pdf). The concentrations of magnesium (Mg), calcium (Ca), manganese (Mn), iron (Fe), cobalt (Co), nickel (Ni), copper (Cu), zinc (Zn) and strontium (Sr) in the digested protein and buffer samples were measured. Data points represent average ± c.v. of eight measurements within two experiments, where c.v. corresponds to coefficient of variance.

One multi-element calibration standard was prepared from concentrated single-element stocks, and used for instrument calibration. The calibration standard was diluted to various concentrations using a solution containing 10% HNO3 and 500 µg/L of Au to cover the expected concentration range of each analyte in the protein sample: 0.01, 0.02, 0.05, 0.1, 0.2 µg/L for Co and Sr; 0.05, 0.1, 0.25, 0.5, 1.0 µg/L for Mn and Ni; 0.25, 0.5, 1.25, 2.5, 5.0 µg/L for Mg and Cu; 0.5, 1.0, 2.5, 5.0, 10.0 µg/L for Fe and Zn; and 2.5, 5.0, 12.5, 25, 50 µg/L for Ca.

The instrument was also calibrated against a set of blank solutions, including commercially available quality controls containing digested hair samples from Public Health Expertise and Reference Center, Quebec (INSPQ, Quebec, Canada), and a water sample containing a broad range of metals from National Institute of Technology (NIST, Gaithersburg, USA).

Special attention was given to correction for matrix-induced interferences. Matrix suppression was compensated by the selection of suitable internal standards, which were matched to masses and, if possible, to ionization properties of the analytes. The internal standards were added to each calibration standard and quality control sample to the same final concentrations as that in the protein sample and buffer (5 µg/L each of Ga and Rh). The elements Mg, Ca, Mn, Fe, Co, Ni, Cu, and Zn were corrected with Ga, while Sr was corrected with Rh. Polyatomic interferences were suppressed with the instrument's DRC

Author Manuscript Author Manuscript Author Manuscript Author Manuscript

technology feature, utilizing ammonia as a second gas for Mn and Fe, while Mg, Ca, Sr, Co, Ni, Cu, and Zn were measured in standard mode without a second gas.

MALDI mass spectrometry

Purified $GABA_{B1b}$-$GABA_{B2}$ complex (0.3 mg/ml, 1 µl) was mixed with 1 µl sinapinic acid matrix solution (Bruker Daltonics, Billerica, USA) containing 10 mg of sinapinic acid in 1 ml of 2.5% trifluoroacetic acid (MilliporeSigma, Burlington, USA) and 50% acetonitrile (MilliporeSigma, Burlington, USA). The protein-matrix suspension (2 µl) was added to the ground steel MALDI target plate and dried at room temperature. Mass spectra were collected using a UltrafleXtreme MALDI-TOF/TOF mass spectrometer (Bruker Daltonic, Billerica, USA) operated with FlexControl software in linear positive mode, i.e. using a mass range of 30,000 to 120,000 daltons. The instrument was externally calibrated with Proteins MALDI-MS calibration kit (MilliporeSigma, Burlington, USA). Each individual mass spectrum was analyzed and adjusted for smoothness and baseline using FlexAnalysis software 3.0 (Bruker Daltonics, Billerica, USA). The molecular mass of the heterodimeric $GABA_{B1b}$-$GABA_{B2}$ complex was determined to be 192,647.967 daltons.

Extended Data

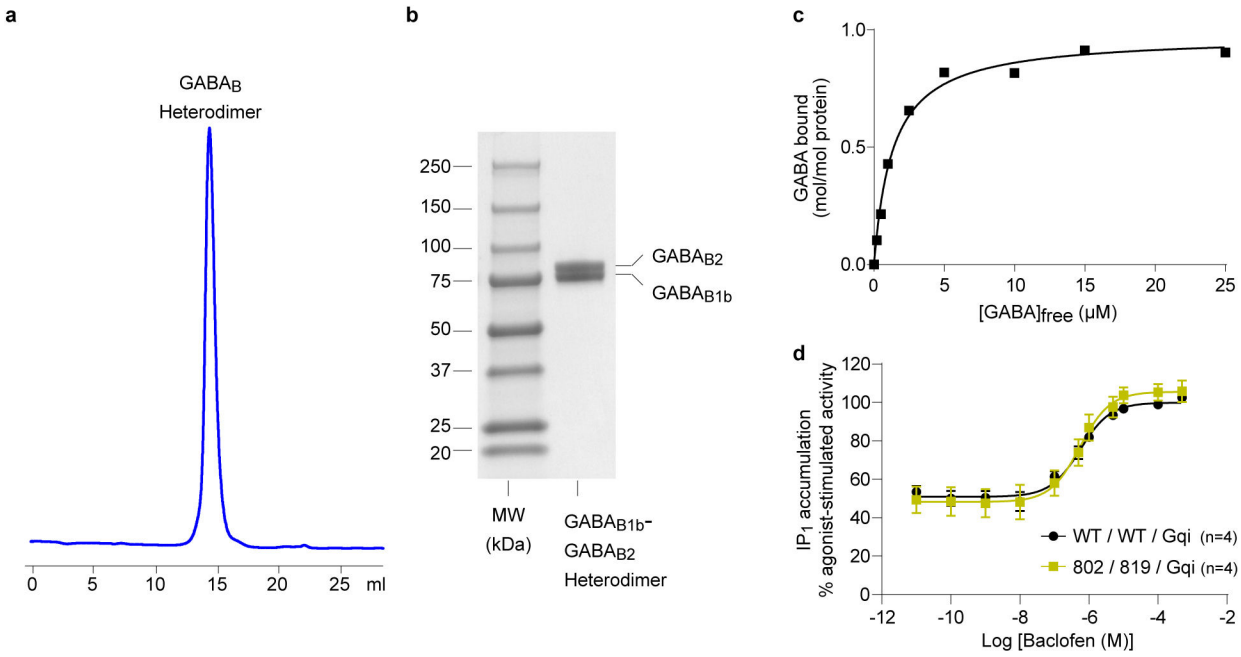

Extended Data Fig. 1 |. Purification and functional analysis of human $GABA_B$ receptor.

a, Superose 6 size exclusion chromatography profile of detergent-purified $GABA_{B1b}$(1–802)-$GABA_{B2}$(1–819) complex.

b, SDS PAGE gel of size exclusion peak fraction from (**a**) under reducing conditions. For gel source data, see Supplementary Fig. 2.

c, Dose-dependent [^{3}H]GABA binding to purified $GABA_{B1b}$(1–802)-$GABA_{B2}$(1–819) complex, reaching maximum molar ratios of GABA-to-receptor binding at 0.98 ± 0.03 mol/mol. Data points represent the mean of triplicate measurements of a typical experiment. The

Author Manuscript Author Manuscript Author Manuscript Author Manuscript

experiment was repeated four times with similar results. Data were subjected to non-linear regression fitting, and the kinetic constants are reported as mean ± s.e.m. of the fit. **d**, Functional analysis comparison of full-length and truncated WT $GABA_B$ receptor. Dose-dependent baclofen-stimulated receptor response in cells transiently expressing $G\alpha_{qi5}$ (abbreviated as Gqi) with full-length $GABA_B$ heterodimer or the C-terminally truncated $GABA_{B1b}$(1–802)-$GABA_{B2}$(1–819) complex. Cells transfected with $G\alpha_{qi5}$ alone were used as negative control. Relative agonist-stimulated activity was measured by IP_1 accumulation and expressed as percentage of maximum wild-type activity induced by baclofen relative to the activity of $G\alpha_{qi5}$ alone. Data points represent average ± s.e.m. of multiple experiments (n), each with quadruplicate measurements. Cell surface expression level was 106% for the $GABA_{B1b}$(1–802)-$GABA_{B2}$(1–819) complex in comparison with the full-length WT/WT heterodimer.

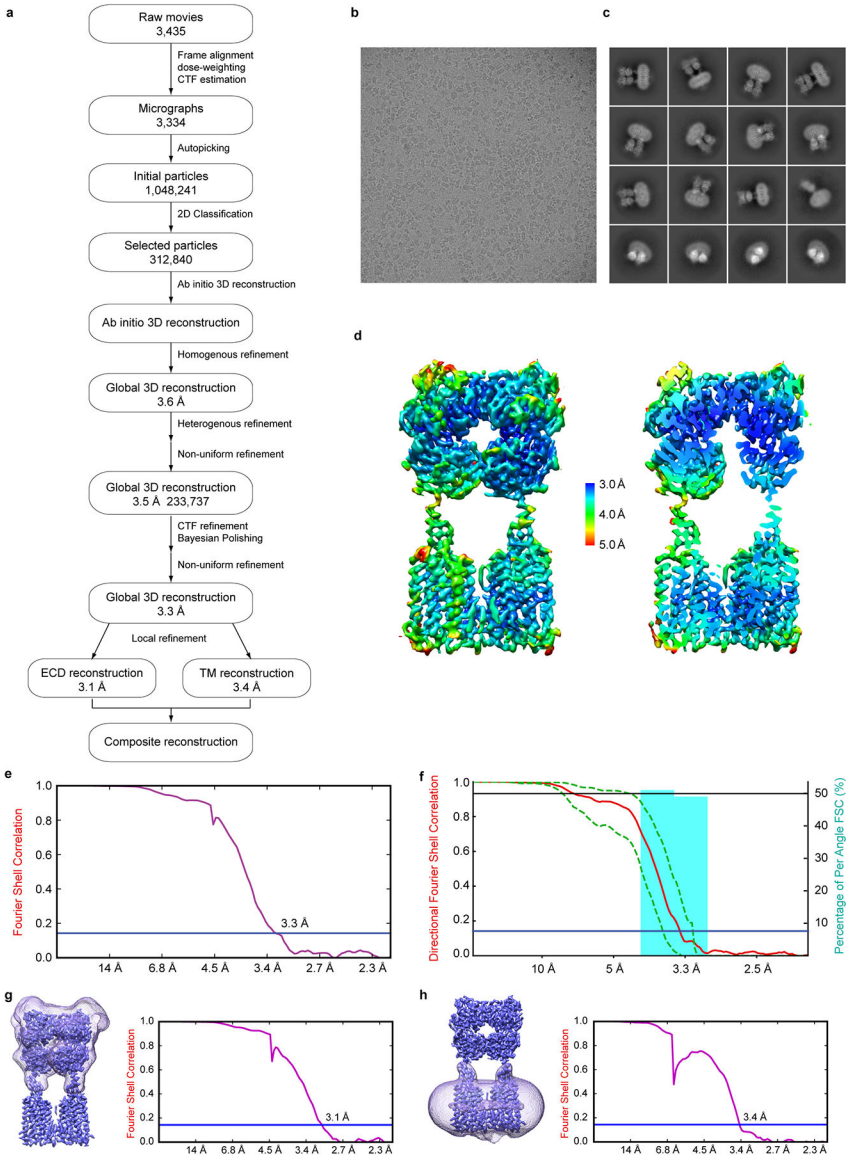

Extended Data Fig. 2 |. Cryo-EM imaging of human $GABA_B$ receptor.

Author Manuscript Author Manuscript Author Manuscript Author Manuscript

a, Workflow of cryo-EM data processing.

b, A representative motion-corrected cryo-electron micrograph of $GABA_B$ receptor.

c, Reference-free 2D class averages highlighting clear density for TM helices.

d, Global density map colored according to local resolution in full and clipped views perpendicular to the plane of the membrane.

e, Global FSC curve (purple) corrected by high-resolution noise substitution. The overall resolution as determined by an FSC cut-off value of 0.143 (blue line) is 3.3 Å.

f, 3D-FSC curves measuring directional resolution anisotropy. Plots show global half-map FSC (red solid line), together with the spread of directional resolution values within ± 1 standard deviation of the mean (area encompassed by green dash lines), and a histogram of 100 such directional resolution values sampled evenly over the 3D-FSC threshold value of 0.143 (blue, right axis). The sphericity value reported by 3D-FSC is 0.958 out of 1.

g,h, Separate FSC curves for the locally refined reconstructions of ECD (**g**) and TM (**h**) domains. Blue line marks the resolution corresponding to an FSC value of 0.143 (ECD: 3.1 Å; TM: 3.4 Å). The inset shows the mask used for each local refinement.

Author Manuscript Author Manuscript Author Manuscript Author Manuscript

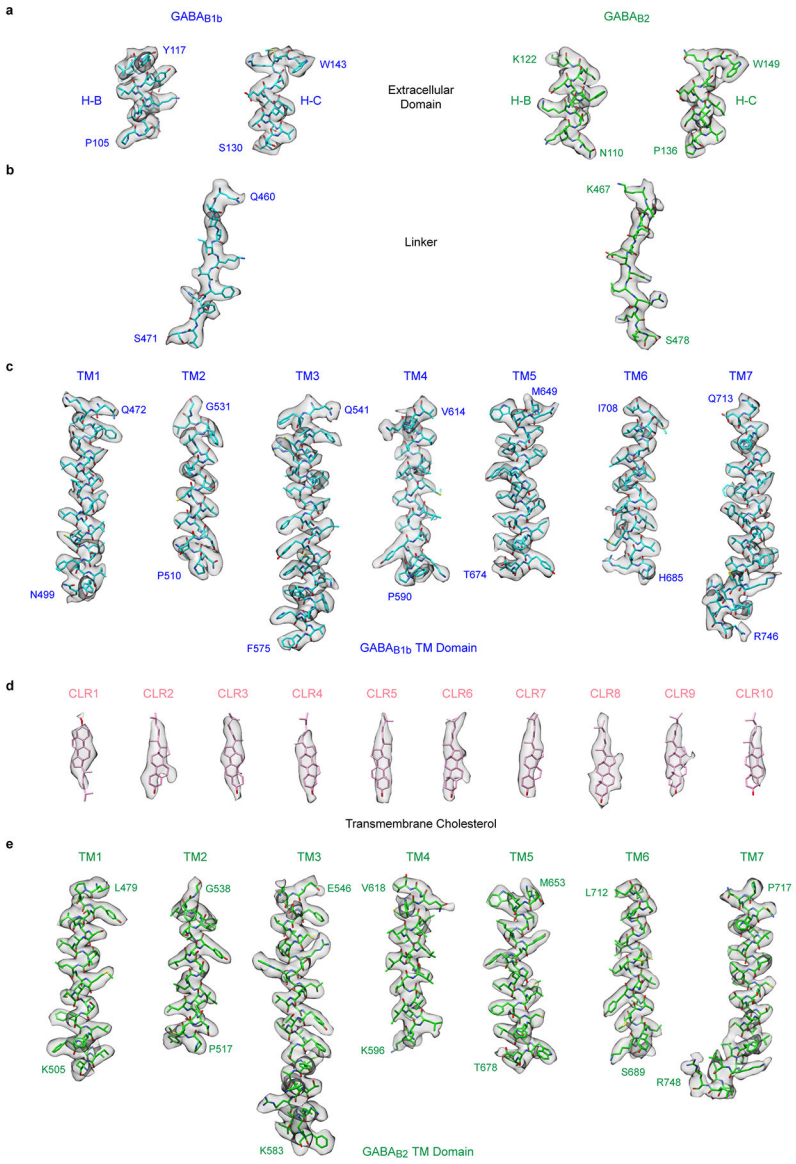

Extended Data Fig. 3 |. Structural model of GABA$_B$ receptor fit within the cryo-EM map.

a-d, Cryo-EM density map and refined model are shown for the LB1 interface helices (H-B and H-C) in the extracellular VFT (**a**), the linker between VFT and TM domain (**b**), all seven TM helices of GABA$_{B1b}$ subunit (**c**) the ten modeled transmembrane cholesterols (**d**) and all seven TM helices of GABA$_{B2}$ subunit (**e**). The density map is a composite of the locally refined reconstructions for the ECD and TM domains. The N- and C-terminal residues of each helix are labeled.

Author Manuscript Author Manuscript Author Manuscript Author Manuscript

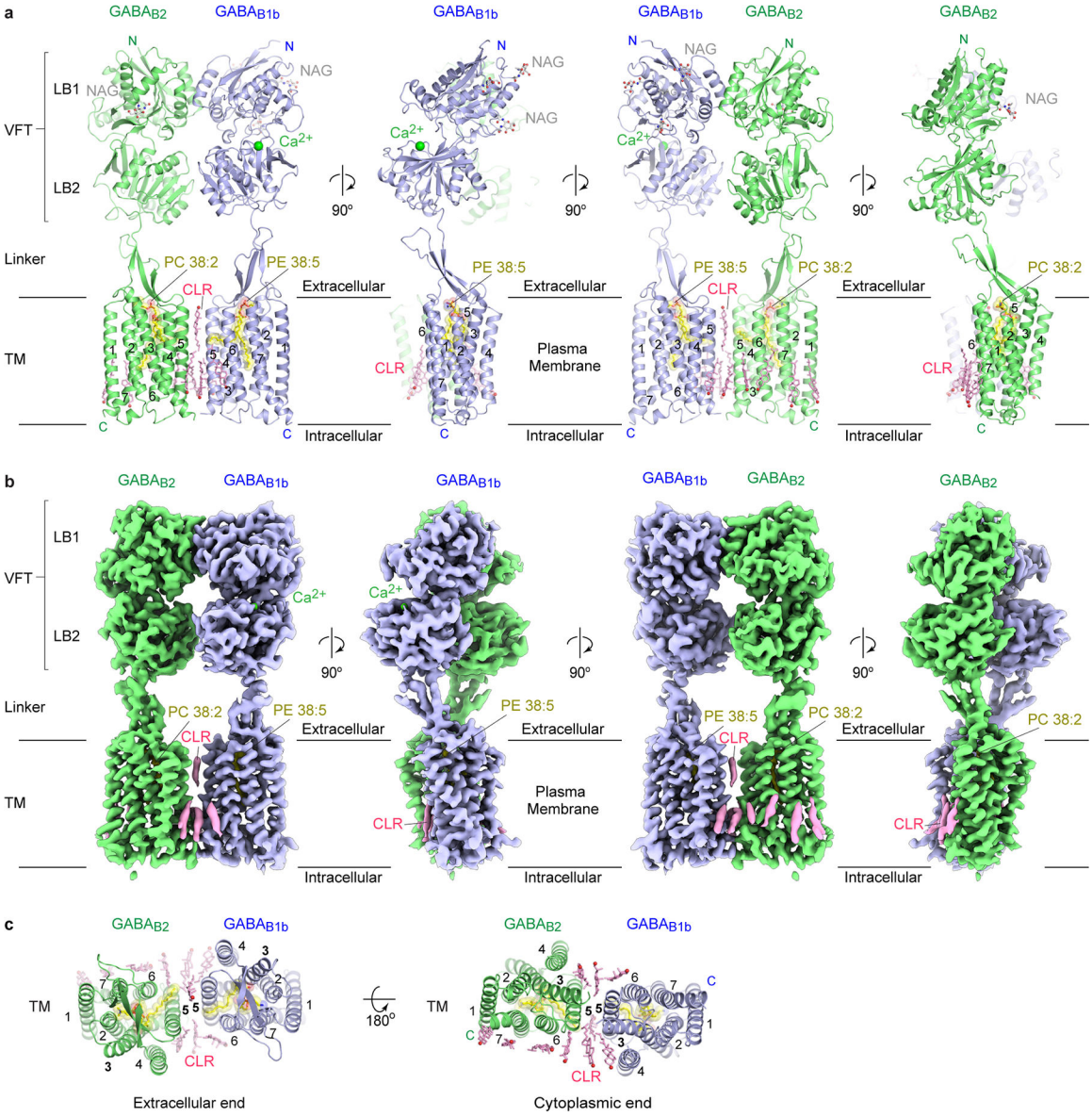

Extended Data Fig. 4 |. Architecture of GABA$_B$ receptor.

a, GABA$_B$ receptor structure in four views related by 90°-rotations about an axis perpendicular to the membrane. GABA$_{B1b}$ (blue) and GABA$_{B2}$ (green) subunits are rendered as cartoon, while Ca^{2+} (green) is shown as a sphere. Phospholipids (PE 38:5 and PC 38:2; yellow) are presented as space-filling models. The observed N-linked glycans (NAG, gray) and cholesterols (CLR, pink) are in ball-and-stick models. TM helices 1 through 7, along with N- and C-termini, are marked for each subunit.

b, Cryo-EM density map of GABA$_B$ receptor, in the same orientation and color scheme as (**a**). The map is composed of local reconstructions for the ECD and TM domains, which were independently refined to 3.1 Å and 3.4 Å, respectively.

c, Linker and TM domain of GABA$_B$ receptor viewed from the extracellular and intracellular sides.

Author Manuscript Author Manuscript Author Manuscript Author Manuscript

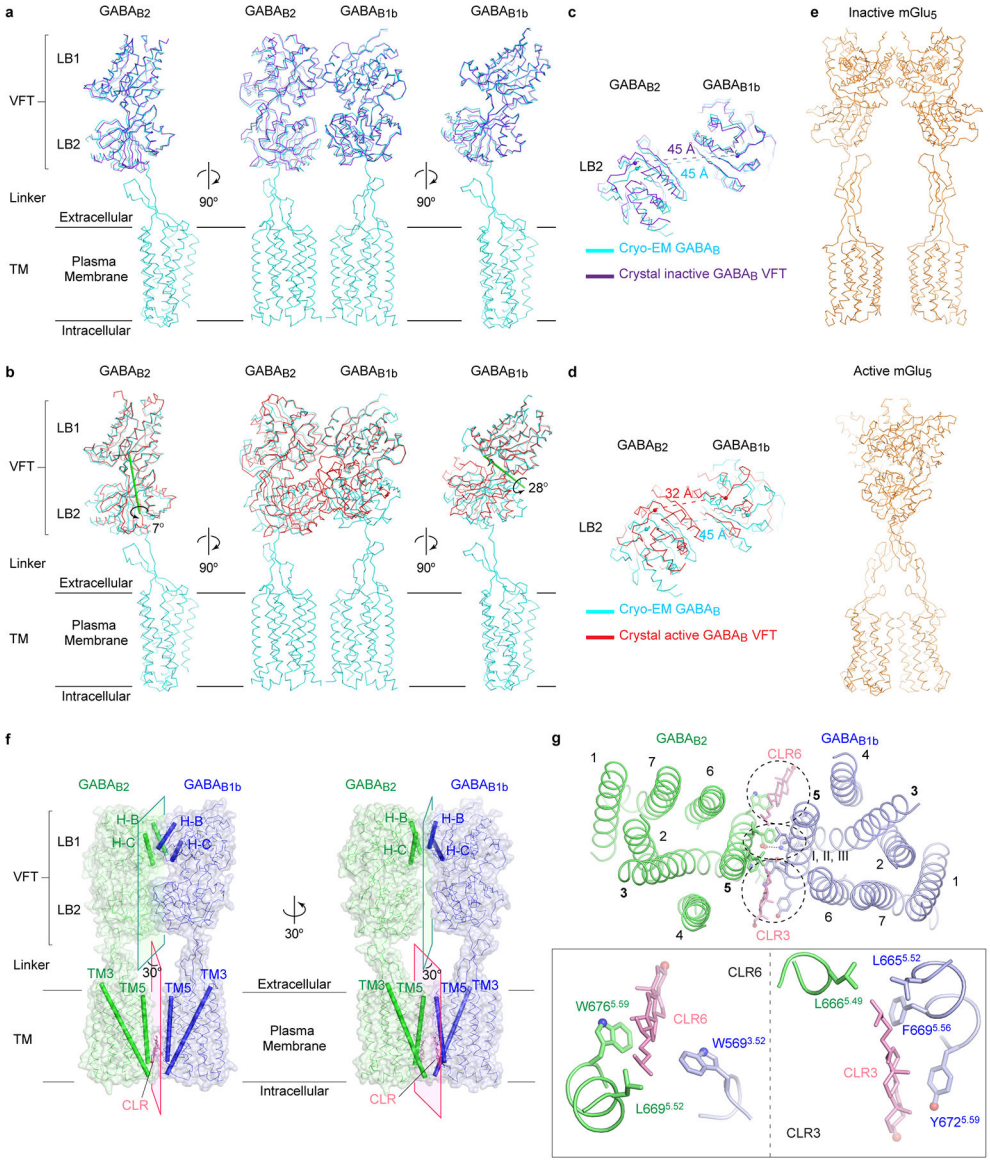

Extended Data Fig. 5 |. Heterodimer conformation and interface features of the GABA$_B$ receptor.

a,b, Cryo-EM structure of near full-length GABA$_B$ receptor (cyan) superimposed with crystal structure of its extracellular VFT module in the inactive-state (PDB code: 4MQE; purple) (**a**) or active state (PDB code: 4MS3; red) (**b**). The middle panel shows the heterodimeric receptor structures superimposed based on the LB1 domain of GABA$_{B1b}$ subunit. The two side panels show superposition of individual GABA$_{B1b}$ and GABA$_{B2}$ subunits based on their respective LB1 domains. In (**b**), Green line denotes the axis of rotation that relates the LB2 domains of near full-length and VFT structures of GABA$_{B1b}$ (rotation χ = 28°, screw translation τ_χ = 0.6 Å), or near full-length and VFT structures of GABA$_{B2}$ (rotation χ = 7°, screw translation τ_χ = 0.3 Å).

c,d, Extracellular LB2 domains viewed from the C-terminal end. Superposition of near full-length (cyan) and extracellular VFT structures (inactive state: purple (**c**); active state; red (**d**)) was based on the LB1 domain of GABA$_{B1b}$ subunit. Within each heterodimeric

Author Manuscript Author Manuscript Author Manuscript Author Manuscript

complex, the C-termini of the LB2 domains in $GABA_{B1b}$ and $GABA_{B2}$ subunits are shown as spheres, and the distance between the two C-termini is marked by a dotted line.

e, Cryo-EM structure of full-length $mGlu_5$ in the inactive (PDB code: 6N52) and active (PDB code: 6N51) conformations[20].

f, Molecular surface of $GABA_{B1b}$-$GABA_{B2}$ complex showing the plane of heterodimer interface for extracellular and TM domains. Structural elements involved in heterodimer formation are highlighted in cartoon (ectodomain: H-B and H-C helices; TM domain: TM5 and TM3 helices).

g, $GABA_B$ TM domain viewed from the extracellular side comparing the locations of core (I, II, IIIa, IIIb) vs. peripheral cholesterol-mediated heterodimer contacts from different layers. Heterodimer contacts mediated by two cholesterols (CLR6, CLR3) are displayed in panels at the bottom.

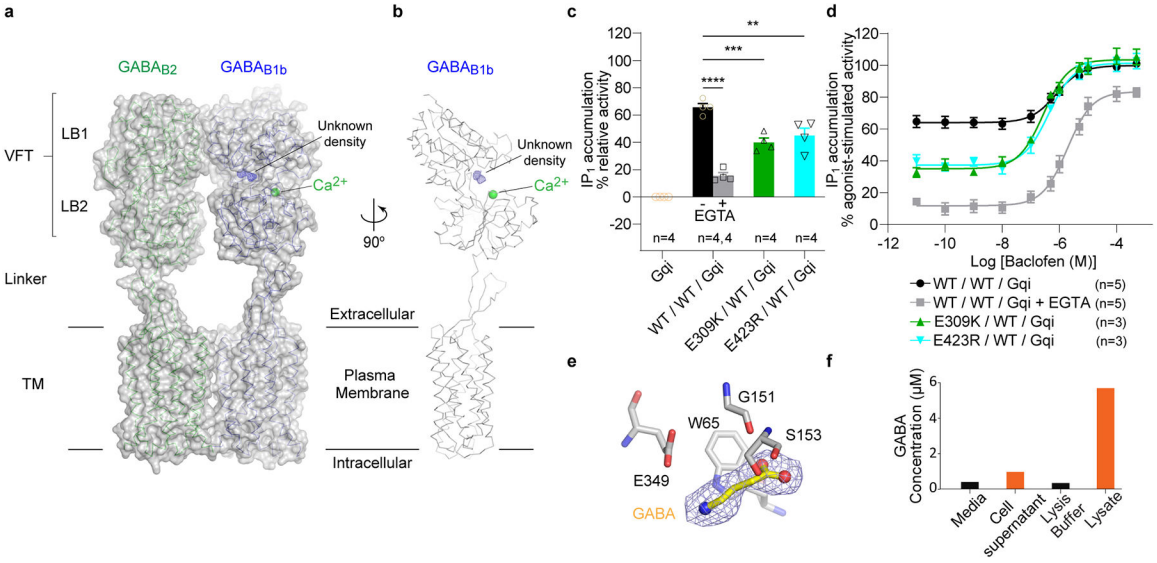

Extended Data Fig. 6 |. Extracellular ligand binding in $GABA_{B1b}$.

a,b, Molecular surface (**a**) and ribbon representation (**b**) of $GABA_{B1b}$ subunit showing the location of Ca^{2+}-binding site and an unmodeled density at the interdomain crevice of VFT.

c,d, Functional analysis of the impact of endogenous Ca^{2+}. Basal activity (**c**) and dose-dependent baclofen-stimulated receptor response (**d**) in cells transiently expressing the $G\alpha_{qi5}$ (abbreviated as Gqi) with different combinations of WT and mutant $GABA_B$ receptor subunits ($GABA_{B1b}$-E309K, abbreviated as E309K; $GABA_{B1b}$-E423R, abbreviated as E423R). IP_1 accumulation of WT/WT heterodimer was measured in the presence and absence of 2.5 mM EGTA. Cells transfected with $G\alpha_{qi5}$ alone were used as negative control. Relative activity in both graphs is expressed as percentage of maximum wild-type activity induced by baclofen relative to the activity of $G\alpha_{qi5}$ alone. Data points represent average ± s.e.m. of multiple experiments (n), each with quadruplicate measurements. ** P=0.0016, ***P=0.0002, **** P<0.0001, one-way ANOVA with Bonferroni's post hoc test was used to calculate statistical differences in basal activity (**c**). Cell surface expression level was 107% for the E309K/WT and 87% for E423R/WT mutants in comparison with the WT/WT heterodimer.

Author Manuscript Author Manuscript Author Manuscript Author Manuscript

e, Fitting of GABA into the extra density (contoured at 7.0 σ) at the orthosteric ligand-binding site and its potential interaction with $GABA_{B1b}$.

f, Concentration of endogenous GABA in the supernatant and lysate of HEK 293 $GnTI^{-}$ cells after recombinant expression of $GABA_B$ receptor, as well as cell culture media and lysis buffer controls, as detected by mass spectrometry.

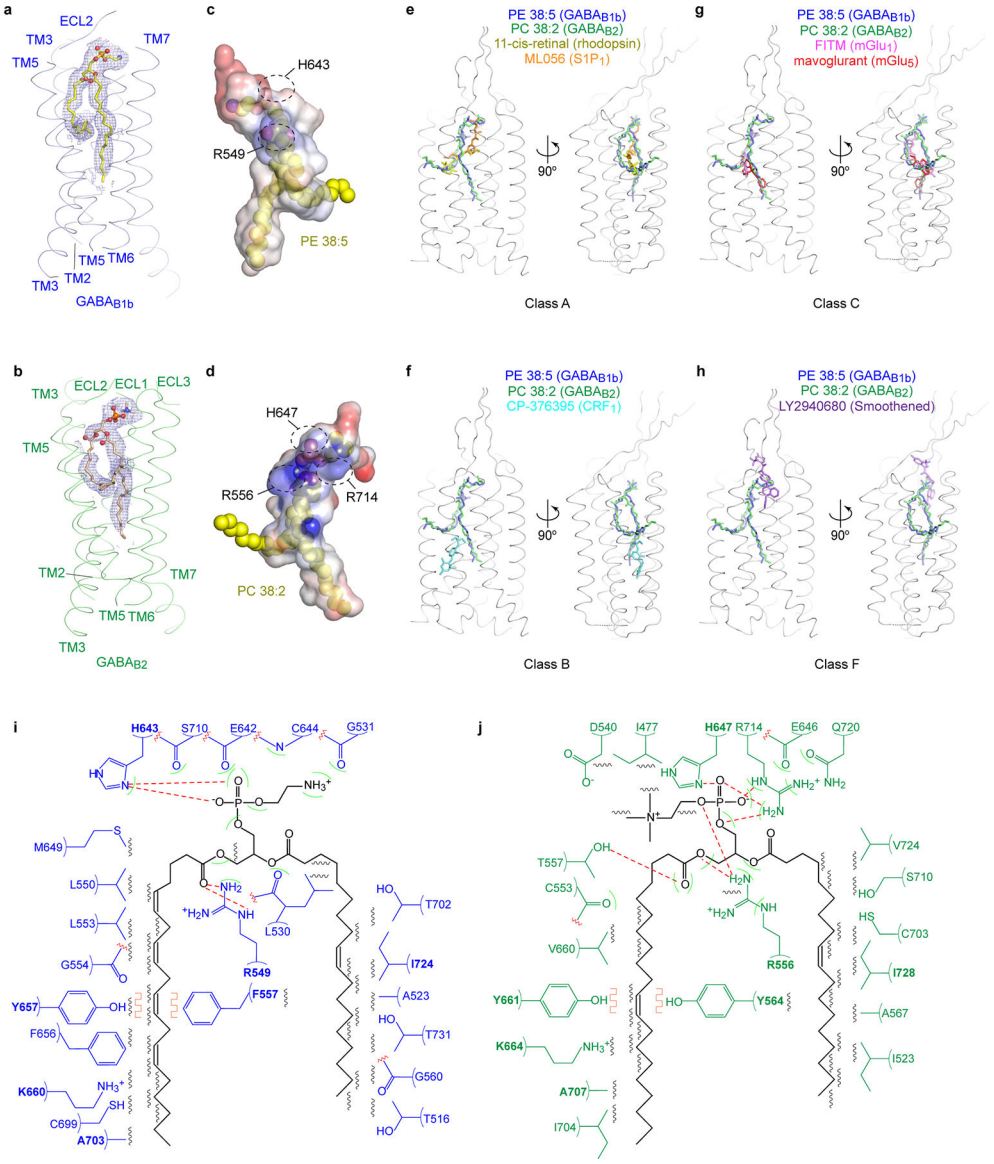

Extended Data Fig. 7 |. Endogenous phospholipid-binding sites of $GABA_B$ receptor.

a,b, Ribbon representation of $GABA_{B1b}$ (**a**) and $GABA_{B2}$ (**b**) TM domain highlighting the cryo-EM density for phospholipids contoured at 4.0 σ. Phospholipids are rendered in ball-and-stick representation.

c,d, Electrostatic potential surface of the lipid-binding pocket in $GABA_{B1b}$ (**c**) and $GABA_{B2}$ (**d**). The phospholipids are shown in sphere models. Charged residues that directly contact the phosphate group of each lipid are marked.

Author Manuscript Author Manuscript Author Manuscript Author Manuscript

e-h, Comparison of phospholipids bound to $GABA_B$ subunits with ligands bound to class A GPCRs rhodopsin[27] (PDB code: 1F88) and $S1P_1$ receptor[24] (PDB code: 3V2Y) (**e**), class B GPCR corticotropin-releasing factor receptor 1[57] (CRF_1; PDB code: 4K5Y) (**f**), class C GPCRs $mGlu_1$[29] (PDB code: 4OR2) and $mGlu_5$[28] (PDB code: 4OO9) (**g**), and class F GPCR smoothened[58] (PDB code: 4JKV) (**h**). In each panel, the Cα trace of $GABA_{B1b}$ linker and TM domain is shown in two orthogonal views in gray, and the superimposed $GABA_B$ ligands PE 38:5 and PC 38:2 are in stick models in blue and green, respectively. Various GPCRs were overlapped onto the TM domain of $GABA_{B1b}$ to bring their bound ligands into superposition

i,j, Schematic diagram of the specific contacts between $GABA_{B1b}$ and PE 38:5 (**i**), and between $GABA_{B2}$ and PC 38:2 (**j**). Selected contacts between residues and phospholipids are highlighted; hydrogen bonds, red dotted lines; hydrophobic contacts, black wiggled lines; polar interactions, green curved lines; pi-stacking interactions, orange box wave. Red zigzags indicate contacting atoms belong to main chain.

Lipid-interacting residues that are conserved in the two subunits are highlighted in bold and include: (1) head group ($GABA_{B1b}$: His643 and $Arg549^{3.32}$; $GABA_{B2}$: His647 and $Arg556^{3.32}$), (2) 20-carbon fatty acyl chain ($GABA_{B1b}$: $Phe557^{3.40}$, $Tyr657^{5.44}$, and $Ala703^{6.54}$; $GABA_{B2}$: $Tyr564^{3.40}$, $Tyr661^{5.44}$, and $Ala707^{6.54}$), (3) 18-carbon fatty acyl chain ($GABA_{B1b}$: $Ile724^{7.36}$; $GABA_{B2}$: $Ile728^{7.36}$).

Author Manuscript Author Manuscript Author Manuscript Author Manuscript

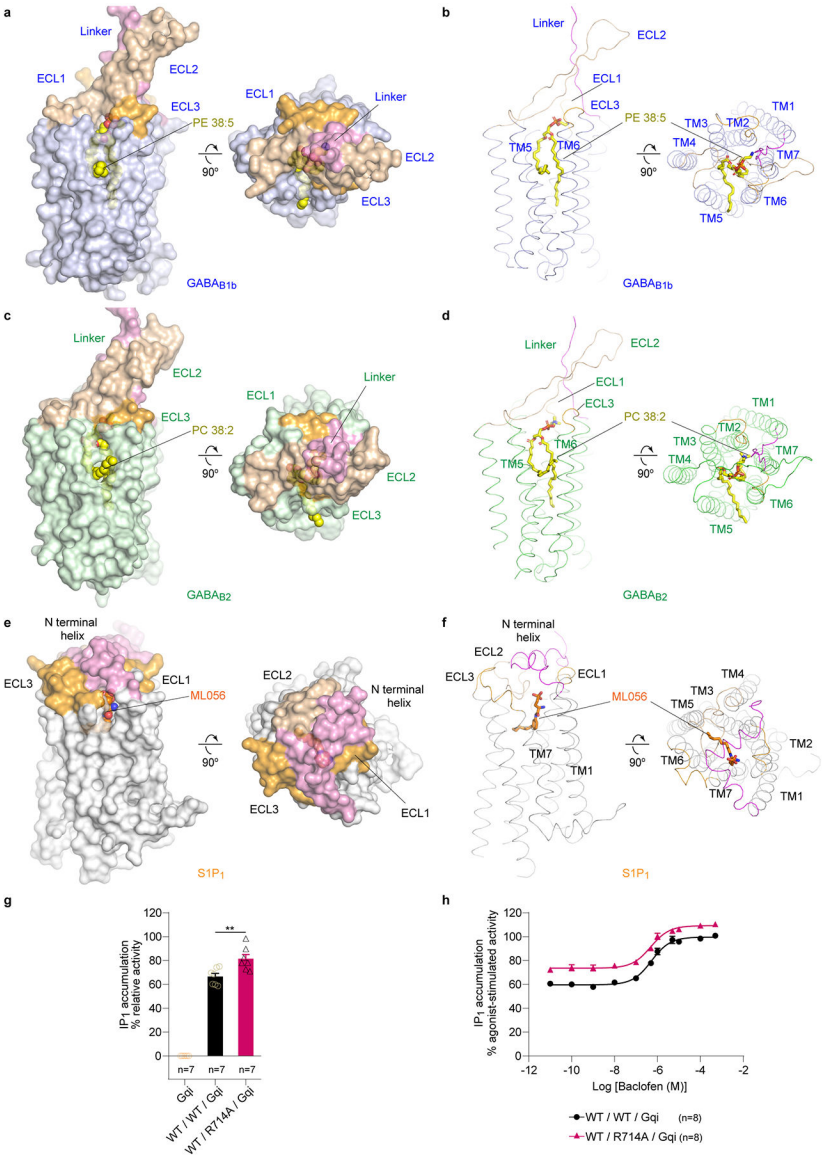

Extended Data Fig. 8 |. Endogenous phospholipid interactions with GABA$_B$ receptor.

a,c,e, Orthogonal views of potential access channel in GABA$_{B1b}$, GABA$_{B2}$, and S1P$_1$ in molecular surface representation, along with phospholipids PE 38:5 and PC 38:2, as well as sphingolipid mimic ML056, respectively, in space-filling representation. Side view (left) shows opening between helices TM5 and TM6 in GABA$_{B1b}$ (**a**) and GABA$_{B2}$ (**c**), and between TM1 and TM7 in S1P$_1$ (**e**), while top view (right) highlights blocked entrance to lipid-binding pocket from the extracellular side. In all cases, ECL1 and ECL3 (orange), ECL2 (pale brown), as well as the linker of GABA$_B$ receptor subunits (purple) and N-terminal helix of S1P$_1$ (purple) are distinguished by color.

b,d,f, The same information presented in (**a, c, e**) but with ribbon model used for GABA$_{B1b}$ (**b**), GABA$_{B2}$ (**d**), and S1P$_1$ (**f**). Lipids are in stick model.

g,h, Functional effect of a GABA$_{B2}$ lipid-binding site mutation. Basal activity (**g**) and dose-dependent baclofen-stimulated receptor response (**h**) in cells transiently expressing Gα_{qi5}

Author Manuscript Author Manuscript Author Manuscript Author Manuscript

(abbreviated as Gqi) with WT $GABA_B$ receptor or WT $GABA_{B1b}$ and mutant $GABA_{B2}$-R714A (abbreviated as R714A) heterodimer. Cells transfected with $G\alpha_{qi5}$ alone were used as negative control. Relative activity in both graphs was measured by IP_1 accumulation, and expressed as percentage of maximum wild-type activity induced by baclofen relative to the activity of $G\alpha_{qi5}$ alone. Data points represent average ± s.e.m. of multiple experiments (n), each with quadruplicate measurements. ** P=0.0016, one-way ANOVA with Bonferroni's post hoc test was used to calculate statistical difference in basal activity (**g**). Cell surface expression level was 77% for the WT/R714A mutant in comparison with the WT/WT heterodimer.

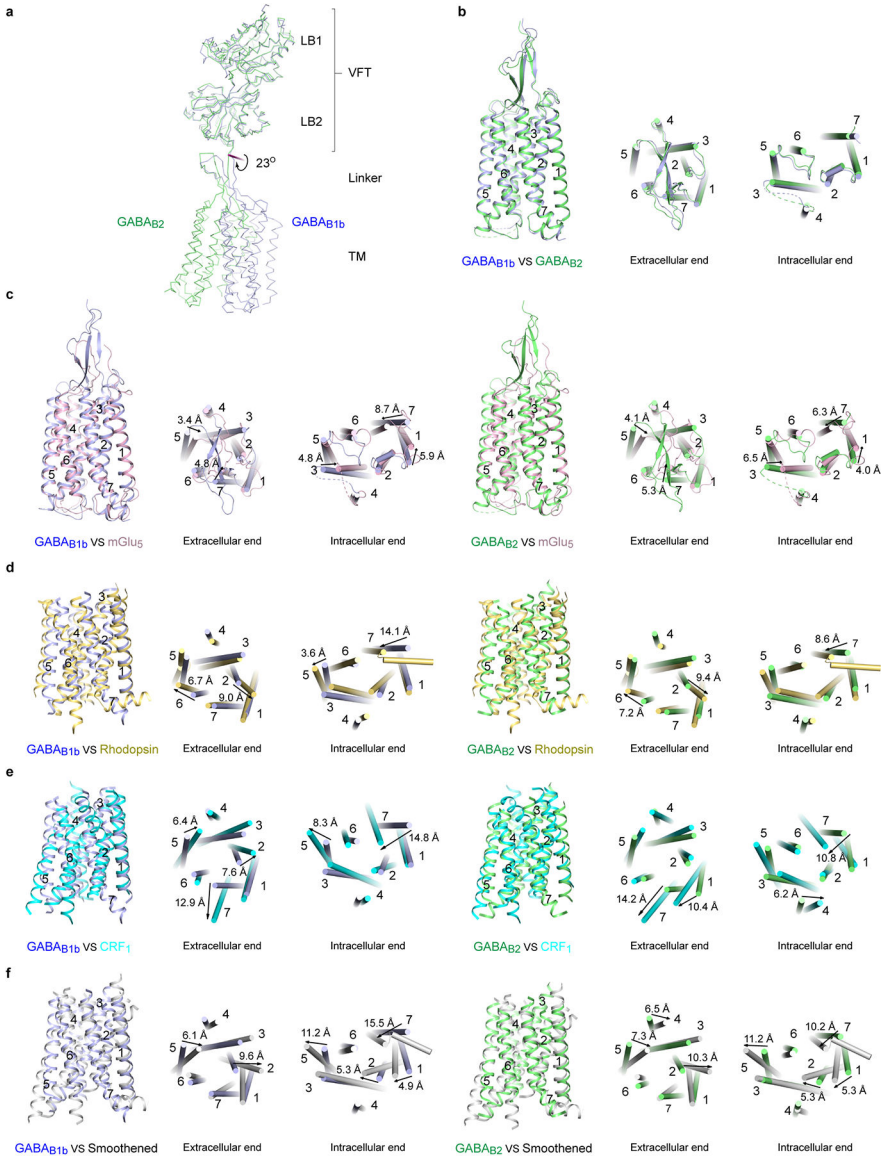

Extended Data Fig. 9 |. Comparison of $GABA_B$ TM domain with other GPCRs.

Author Manuscript Author Manuscript Author Manuscript Author Manuscript

a, Superposition of $GABA_{B1b}$ and $GABA_{B2}$ subunits based on their VFT modules. Purple line denotes the axis of rotation that relates the linker and TM domains of $GABA_{B1b}$ and $GABA_{B2}$ (rotation χ = 23°, screw translation τ_χ = 0.01 Å).
b, Superposition of the linker and TM domains of $GABA_{B1b}$ and $GABA_{B2}$ subunits.
c, Superposition of the linker and TM domains of each $GABA_B$ subunit with class C GPCR $mGlu_5$[20] (PDB code: 6N52) in three different views, with arrows revealing inward extracellular shifts in TM5 and 7, as well as an inward intracellular shift in TM3, in $mGlu_5$ compared to either $GABA_B$ subunit.
d-f, Superposition of the TM helices of each $GABA_B$ subunit with the class A GPCR rhodopsin[27] (PDB code: 1F88) (**d**), class B GPCR CRF_1[57] (PDB code: 4K5Y) (**e**), and class F GPCR smoothened[58] (PDB code: 4JKV) (**f**). Arrows indicate large shifts in TM helix positions between $GABA_B$ subunits and other GPCRs, such as outward extracellular movements in class A (TM2 and 6), class B (TM1, 2, and 7), and class F (TM2, 4, and 5). There are also inward intracellular shifts in TM7 in all comparisons, and outward intracellular shifts in TM5 in class A, B and F.

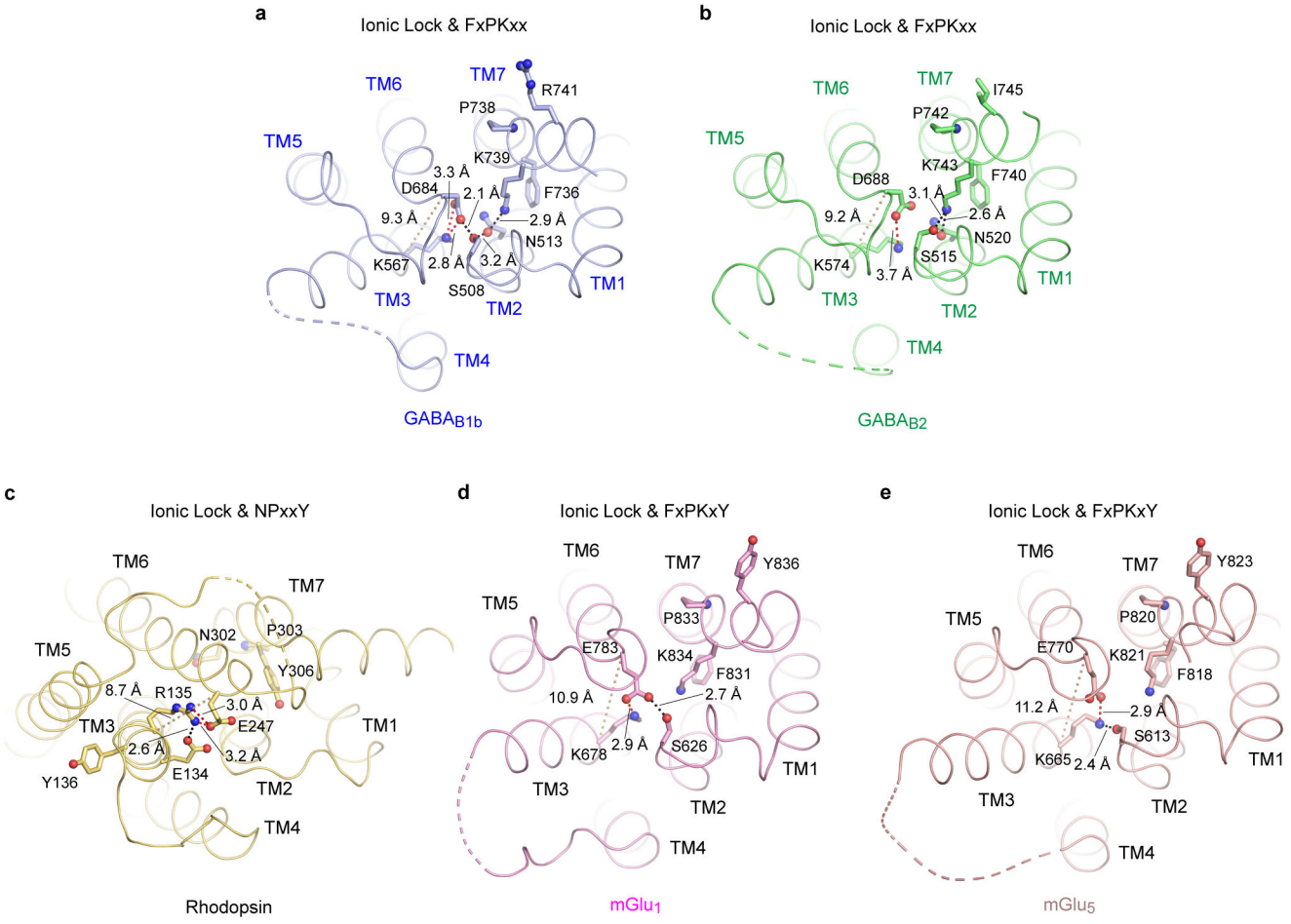

Extended Data Fig. 10 |. Conserved motifs in $GABA_B$, rhodopsin and mGlu receptors.
a,b, The ′ionic lock′ and FxPKxx motifs in $GABA_{B1b}$ (**a**) and $GABA_{B2}$ (**b**) subunits. The ′ionic locks′ consist of Asp684 of ICL3 and $Lys567^{3.50}$ in $GABA_{B1b}$ and Asp688 of ICL3

Author Manuscript Author Manuscript Author Manuscript Author Manuscript

and Lys574$^{3.50}$ in $GABA_{B2}$. The FxPKxx motifs include the conserved Lys739$^{7.51}$ of $GABA_{B1b}$ and Lys743$^{7.51}$ of $GABA_{B2}$, which interact with the ′ionic locks′ through Asn$^{2.39}$ ($GABA_{B1b}$-N513$^{2.39}$; $GABA_{B2}$-N520$^{2.39}$) and a serine ($GABA_{B1b}$-S508; $GABA_{B2}$-S515) in ICL1.

c, The ′ionic lock′ and NPxxY motifs in class A rhodopsin[27].

d,e, The ′ionic lock′ and FxPKxY motifs in class C receptors $mGlu_1$[29] (**d**) and $mGlu_5$[28] (**e**), which are in close proximity as in $GABA_B$ subunits.

Key residues of the motifs are displayed in stick models. Hydrogen bonds are indicated by black dotted lines. Interactions between participating residues of the ′ionic lock′ are denoted by red dotted lines with distances labeled. Distances between the Cα atoms of the ′ionic lock′ residues are marked by brown dotted lines.

Supplementary Material

Refer to Web version on PubMed Central for supplementary material.

Acknowledgments:

We thank Dr. Richard Henderson for early-stage cryo-EM investigation and critical reading of the manuscript, Dr. Charles S. Zuker for advice and financial support, Dr. Charles Karan and Ronald Realubit for assistance with the EnVision plate reader at Columbia Genome Center, Drs. Alexander Sobolevsky, Kei Saotome, and Erhu Cao for the gift of BacMam vectors, Dr. Yung H. Wong for the plasmid of a $G\alpha_{qi5}$ chimera, Drs. Brian K. Kobilka and Georgios Skiniotis for advice. Titan Krios data collectionwas performed at the Simons Electron Microscopy Center, directed by Dr. Bridget O. Carragher and Clint Potter, supported by grants from the Simons Foundation (SF349247), NYSTAR, and NIH (GM103310). This work was supported by NIH grants R01GM088454 (to Q.R.F.), R01GM125801 (to Q.R.F., P.A.S., M.Q.), R01GM107462 (to W.A.H.), P41GM116799 (to W.A.H.), and U2C ES030158 for lipid identification (to O.F.). Q.R.F. was an Irma Hirschl Career Scientist, Pew Scholar, McKnight Scholar and Schaefer Scholar.

References

1. Bettler B, Kaupmann K, Mosbacher J & Gassmann M Molecular structure and physiological functions of GABA(B) receptors. Physiol. Rev 84, 835–867, (2004). [PubMed: 15269338]
2. Jones KA et al. GABA(B) receptors function as a heteromeric assembly of the subunits GABA(B)R1 and GABA(B)R2. Nature 396, 674–679, (1998). [PubMed: 9872315]
3. Kaupmann K et al. GABA(B)-receptor subtypes assemble into functional heteromeric complexes. Nature 396, 683–687, (1998). [PubMed: 9872317]
4. White JH et al. Heterodimerization is required for the formation of a functional GABA(B) receptor. Nature 396, 679–682, (1998). [PubMed: 9872316]
5. Kuner R et al. Role of heteromer formation in $GABA_B$ receptor function. Science 283, 74–77, (1999). [PubMed: 9872744]
6. Ng GY et al. Identification of a $GABA_B$ receptor subunit, gb2, required for functional GABAB receptor activity. J. Biol. Chem 274, 7607–7610, (1999). [PubMed: 10075644]
7. Kaupmann K et al. Expression cloning of GABA(B) receptors uncovers similarity to metabotropic glutamate receptors. Nature 386, 239–246, (1997). [PubMed: 9069281]
8. Malitschek B et al. The N-terminal domain of gamma-aminobutyric Acid(B) receptors is sufficient to specify agonist and antagonist binding. Mol. Pharmacol 56, 448–454, (1999). [PubMed: 10419566]
9. Galvez T et al. Allosteric interactions between GB1 and GB2 subunits are required for optimal GABA(B) receptor function. EMBO J. 20, 2152–2159, (2001). [PubMed: 11331581]
10. Margeta-Mitrovic M, Jan YN & Jan LY Function of GB1 and GB2 subunits in G protein coupling of GABA(B) receptors. Proc. Natl. Acad. Sci. U. S. A 98, 14649–14654, (2001). [PubMed: 11724956]

Author Manuscript Author Manuscript Author Manuscript Author Manuscript

11. Robbins MJ et al. GABA(B2) is essential for g-protein coupling of the GABA(B) receptor heterodimer. J. Neurosci 21, 8043–8052, (2001). [PubMed: 11588177]
12. Duthey B et al. A single subunit (GB2) is required for G-protein activation by the heterodimeric GABA(B) receptor. J. Biol. Chem 277, 3236–3241, (2002). [PubMed: 11711539]
13. Havlickova M et al. The intracellular loops of the GB2 subunit are crucial for G-protein coupling of the heteromeric gamma-aminobutyrate B receptor. Mol. Pharmacol 62, 343–350, (2002). [PubMed: 12130687]
14. Monnier C et al. Trans-activation between 7TM domains: implication in heterodimeric GABA(B) receptor activation. EMBO J. 30, 32–42, (2011). [PubMed: 21063387]
15. Pin JP & Bettler B Organization and functions of mGlu and GABAB receptor complexes. Nature 540, 60–68, (2016). [PubMed: 27905440]
16. Geng Y, Bush M, Mosyak L, Wang F & Fan QR Structural mechanism of ligand activation in human GABA(B) receptor. Nature 504, 254–259, (2013). [PubMed: 24305054]
17. Burmakina S, Geng Y, Chen Y & Fan QR Heterodimeric coiled-coil interactions of human GABAB receptor. Proc. Natl. Acad. Sci. U. S. A 111, 6958–6963, (2014). [PubMed: 24778228]
18. Conklin BR, Farfel Z, Lustig KD, Julius D & Bourne HR Substitution of three amino acids switches receptor specificity of Gq alpha to that of Gi alpha. Nature 363, 274–276, (1993). [PubMed: 8387644]
19. Xue L et al. Rearrangement of the transmembrane domain interfaces associated with the activation of a GPCR hetero-oligomer. Nat Commun 10, 2765, (2019). [PubMed: 31235691]
20. Koehl A et al. Structural insights into the activation of metabotropic glutamate receptors. Nature 566, 79–84, (2019). [PubMed: 30675062]
21. Geng Y et al. Structural mechanism of ligand activation in human calcium-sensing receptor. Elife 5, (2016).
22. Galvez T et al. Ca(2+) requirement for high-affinity gamma-aminobutyric acid (GABA) binding at GABA(B) receptors: involvement of serine 269 of the GABA(B)R1 subunit. Mol. Pharmacol 57, 419–426, (2000). [PubMed: 10692480]
23. Wise A et al. Calcium sensing properties of the GABA(B) receptor. Neuropharmacology 38, 1647–1656, (1999). [PubMed: 10587080]
24. Hanson MA et al. Crystal structure of a lipid G protein-coupled receptor. Science 335, 851–855, (2012). [PubMed: 22344443]
25. Rasmussen SG et al. Crystal structure of the beta2 adrenergic receptor-Gs protein complex. Nature 477, 549–555, (2011). [PubMed: 21772288]
26. Thal DM, Glukhova A, Sexton PM & Christopoulos A Structural insights into G-protein-coupled receptor allostery. Nature 559, 45–53, (2018). [PubMed: 29973731]
27. Palczewski K et al. Crystal structure of rhodopsin: A G protein-coupled receptor. Science 289, 739–745, (2000). [PubMed: 10926528]
28. Dore AS et al. Structure of class C GPCR metabotropic glutamate receptor 5 transmembrane domain. Nature 511, 557–562, (2014). [PubMed: 25042998]
29. Wu H et al. Structure of a class C GPCR metabotropic glutamate receptor 1 bound to an allosteric modulator. Science 344, 58–64, (2014). [PubMed: 24603153]

Methods references

30. Goehring A et al. Screening and large-scale expression of membrane proteins in mammalian cells for structural studies. Nat. Protoc 9, 2574–2585, (2014). [PubMed: 25299155]
31. Margeta-Mitrovic M, Jan YN & Jan LY A trafficking checkpoint controls GABA(B) receptor heterodimerization. Neuron 27, 97–106, (2000). [PubMed: 10939334]
32. Pagano A et al. C-terminal interaction is essential for surface trafficking but not for heteromeric assembly of GABA(b) receptors. J. Neurosci 21, 1189–1202, (2001). [PubMed: 11160389]
33. Reeves PJ, Callewaert N, Contreras R & Khorana HG Structure and function in rhodopsin: high-level expression of rhodopsin with restricted and homogeneous N-glycosylation by a tetracycline-

Author Manuscript Author Manuscript Author Manuscript Author Manuscript

inducible N-acetylglucosaminyltransferase I-negative HEK293S stable mammalian cell line. Proc. Natl. Acad. Sci. U. S. A 99, 13419–13424, (2002). [PubMed: 12370423]

34. Zheng SQ et al. MotionCor2: anisotropic correction of beam-induced motion for improved cryo-electron microscopy. Nat Methods 14, 331–332, (2017). [PubMed: 28250466]
35. Scheres SH RELION: implementation of a Bayesian approach to cryo-EM structure determination. J. Struct. Biol 180, 519–530, (2012). [PubMed: 23000701]
36. Zhang K Gctf: Real-time CTF determination and correction. J. Struct. Biol 193, 1–12, (2016). [PubMed: 26592709]
37. Punjani A, Rubinstein JL, Fleet DJ & Brubaker MA cryoSPARC: algorithms for rapid unsupervised cryo-EM structure determination. Nat Methods 14, 290–296, (2017). [PubMed: 28165473]
38. Scheres SH & Chen S Prevention of overfitting in cryo-EM structure determination. Nat Methods 9, 853–854, (2012). [PubMed: 22842542]
39. Tan YZ et al. Addressing preferred specimen orientation in single-particle cryo-EM through tilting. Nat Methods 14, 793–796, (2017). [PubMed: 28671674]
40. Pettersen EF et al. UCSF Chimera--a visualization system for exploratory research and analysis. J. Comput. Chem 25, 1605–1612, (2004). [PubMed: 15264254]
41. Punjani A & Fleet DJ 3D Variability Analysis: Directly resolving continuous flexibility and discrete heterogeneity from single particle cryo-EM images. bioRxiv, (2020).
42. Emsley P, Lohkamp B, Scott WG & Cowtan K Features and development of Coot. Acta Crystallogr. D Biol. Crystallogr 66, 486–501, (2010). [PubMed: 20383002]
43. Adams PD et al. PHENIX: a comprehensive Python-based system for macromolecular structure solution. Acta Crystallogr. D Biol. Crystallogr 66, 213–221, (2010). [PubMed: 20124702]
44. Chen VB et al. MolProbity: all-atom structure validation for macromolecular crystallography. Acta Crystallogr. D Biol. Crystallogr 66, 12–21, (2010). [PubMed: 20057044]
45. Barad BA et al. EMRinger: side chain-directed model and map validation for 3D cryo-electron microscopy. Nat Methods 12, 943–946, (2015). [PubMed: 26280328]
46. Novotny M, Madsen D & Kleywegt GJ Evaluation of protein fold comparison servers. Proteins 54, 260–270, (2004). [PubMed: 14696188]
47. Goddard TD et al. UCSF ChimeraX: Meeting modern challenges in visualization and analysis. Protein Sci. 27, 14–25, (2018). [PubMed: 28710774]
48. Morin A et al. Collaboration gets the most out of software. Elife 2, e01456, (2013). [PubMed: 24040512]
49. Geng Y et al. Structure and functional interaction of the extracellular domain of human GABA(B) receptor GBR2. Nat. Neurosci 15, 970–978, (2012). [PubMed: 22660477]
50. Quick M & Javitch JA Monitoring the function of membrane transport proteins in detergent-solubilized form. Proc. Natl. Acad. Sci. U. S. A 104, 3603–3608, (2007). [PubMed: 17360689]
51. Gupta K et al. Identifying key membrane protein lipid interactions using mass spectrometry. Nat. Protoc 13, 1106–1120, (2018). [PubMed: 29700483]
52. Mafu S et al. Biosynthesis of the microtubule-destabilizing diterpene pseudolaric acid B from golden larch involves an unusual diterpene synthase. Proc. Natl. Acad. Sci. U. S. A 114, 974–979, (2017). [PubMed: 28096378]
53. Kind T et al. LipidBlast in silico tandem mass spectrometry database for lipid identification. Nat Methods 10, 755–758, (2013). [PubMed: 23817071]
54. Mukherjee RS, McBride EW, Beinborn M, Dunlap K & Kopin AS Point mutations in either subunit of the GABAB receptor confer constitutive activity to the heterodimer. Mol. Pharmacol 70, 1406–1413, (2006). [PubMed: 16847143]
55. Chen KLB, Amarasiriwardena CJ & Christiani DC Determination of total arsenic concentrations in nails by inductively coupled plasma mass spectrometry.. Biol. Trace Elem. Res 67, 109–125, (1999). [PubMed: 10073418]
56. Pruszkowski E, Neubauer K & Thomas R An Overview of Clinical Applications by Inductively Coupled Plasma Mass Spectrometry.. At. Spectrosc 19, 111–115, (1998).

Author Manuscript Author Manuscript Author Manuscript Author Manuscript

57. Hollenstein K et al. Structure of class B GPCR corticotropin-releasing factor receptor 1. Nature 499, 438–443, (2013). [PubMed: 23863939]

58. Wang C et al. Structure of the human smoothened receptor bound to an antitumour agent. Nature 497, 338–343, (2013). [PubMed: 23636324]

Author Manuscript Author Manuscript Author Manuscript Author Manuscript

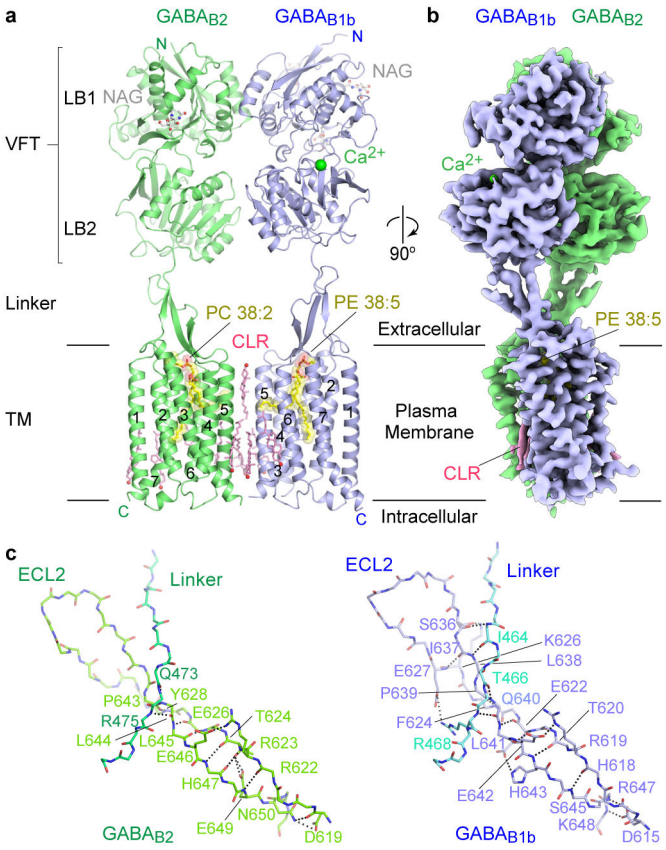

Fig. 1 |. Cryo-EM structure of human GABA$_B$ receptor.

a, Ribbon representation of GABA$_B$ receptor structure composed of GABA$_{B1b}$ (blue) and GABA$_{B2}$ (green) subunits. Ca^{2+} (green): sphere. Phospholipids (PE 38:5; PC 38:2; yellow): space-filling models. N-linked glycans (NAG, gray) and cholesterols (CLR, pink): ball-and-stick models. TM helices 1 through 7 are marked for each subunit.

b, Cryo-EM density map of GABA$_B$ receptor composed of local reconstructions for extracellular (3.1 Å) and TM (3.4 Å) domains, in an orthogonal view from (**a**).

c, Linker domains of GABA$_{B1b}$ and GABA$_{B2}$, showing the main-chain and side-chain hydrogen-bonding patterns between linker region and ECL2.

Author Manuscript Author Manuscript Author Manuscript Author Manuscript

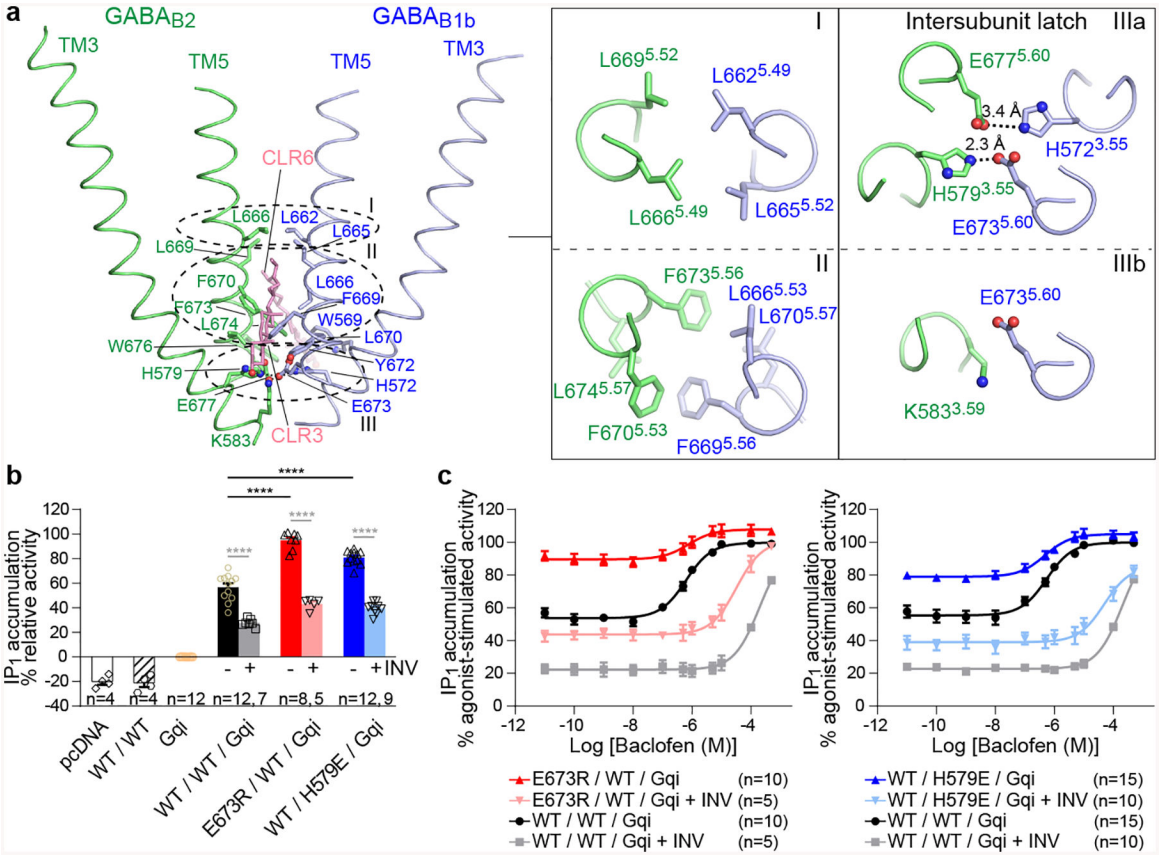

Fig. 2 |. Transmembrane heterodimer interface of $GABA_B$ receptor.

a, TM heterodimer interface formed by TM5 and TM3 of both subunits. Three layers (I, II, III) of interfacial contacts are identified by dotted circles. Direct heterodimer contacts within each layer are displayed in panels on the right.

b,c, Functional analysis of the ′intersubunit latch′. Basal activity (**b**) and dose-dependent baclofen-stimulated receptor response (**c**) in cells transiently expressing the $G\alpha_{qi5}$ chimera protein (abbreviated as Gqi) with different combinations of wild-type (WT) and mutant $GABA_B$ subunits ($GABA_{B1b}$-E673R, abbreviated as E673R; $GABA_{B2}$-H579E, abbreviated as H579E). IP_1 accumulation was measured in the presence and absence of 20 μM CGP54626 (abbreviated as INV). Cells transfected with empty pcDNA3.1 vector, $G\alpha_{qi5}$ alone, or WT $GABA_B$ subunits in the absence of $G\alpha_{qi5}$ were used as controls. Relative activity is expressed as percentage of maximum wild-type activity induced by baclofen relative to the activity of $G\alpha_{qi5}$ alone. Data points represent average ± s.e.m. of multiple experiments (n), each with quadruplicate measurements. ****P<0.0001, one-way ANOVA with Bonferroni's post hoc test was used to calculate statistical differences in basal activity (**b**). Cell surface expression level was 90% for the E673R/WT and 76% for WT/H579E mutants in comparison with the WT/WT heterodimer.

Author Manuscript Author Manuscript Author Manuscript Author Manuscript

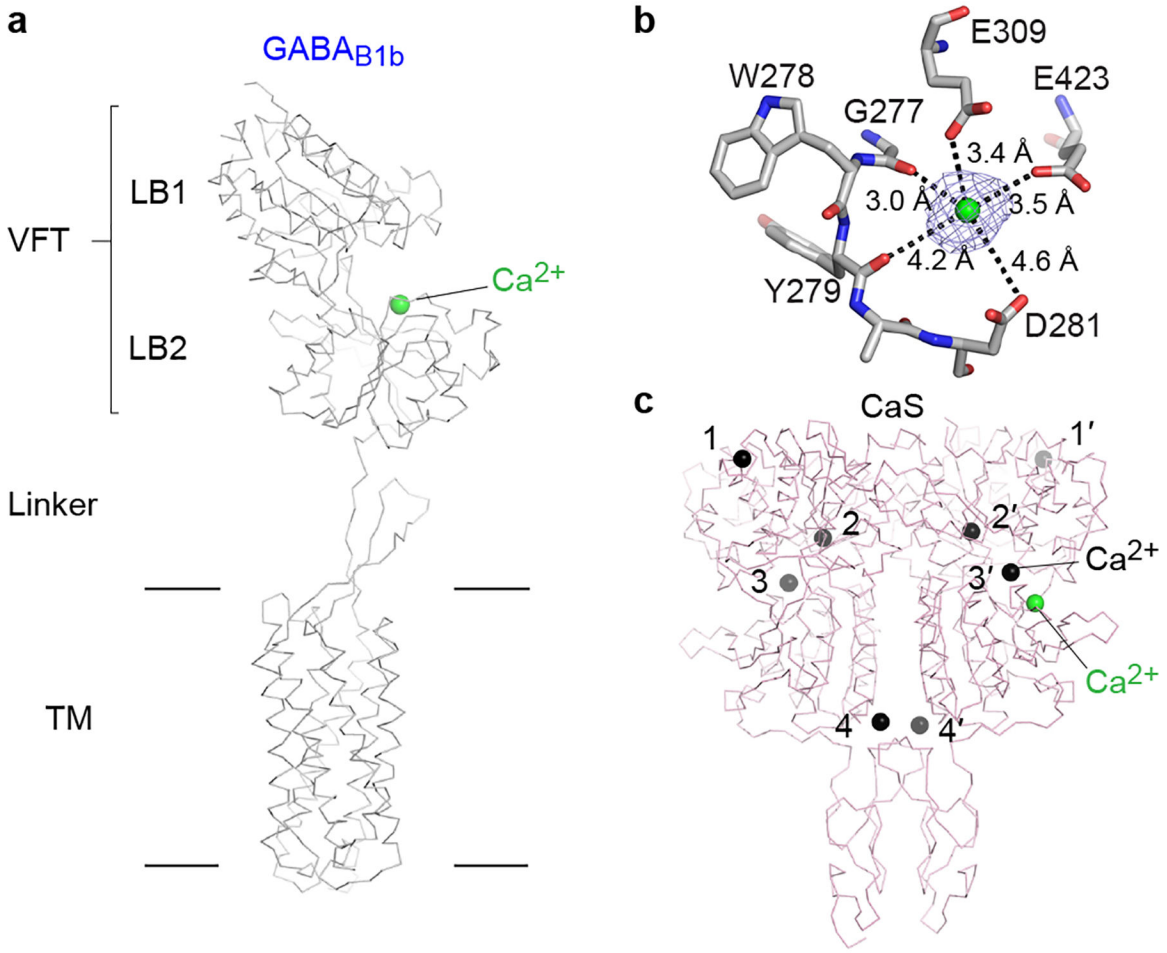

Fig. 3 |. Ca^{2+} binding in $GABA_{B1b}$.

a, Ribbon representation of $GABA_{B1b}$ subunit showing the location of Ca^{2+}-binding site at the interdomain crevice of VFT.

b, Specific interactions between $GABA_{B1b}$ and Ca^{2+}. Mesh represents the cryo-EM density map contoured at 7.5 σ surrounding Ca^{2+}.

c, CaS receptor ECD crystal structure (PDB code: 5K5S) highlighting its bound Ca^{2+} (black spheres, numbered 1–4 and 1′−4′ in the two protomers) and the corresponding location of the Ca^{2+}-binding site in $GABA_{B1b}$ (green sphere).

Author Manuscript Author Manuscript Author Manuscript Author Manuscript

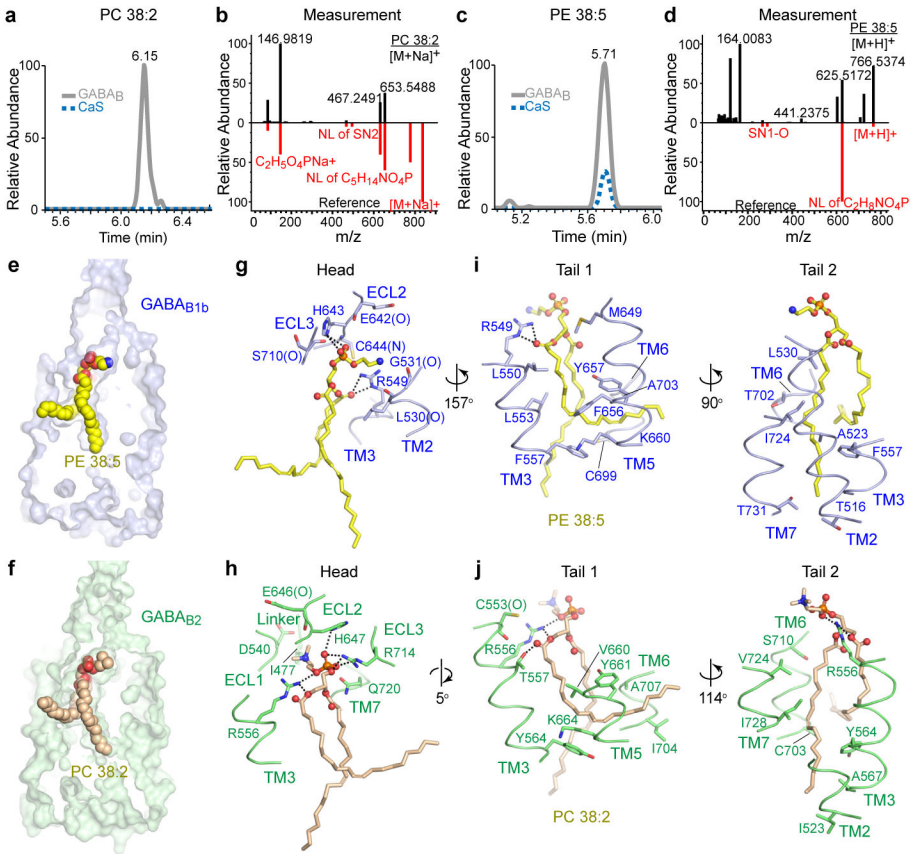

Fig. 4 |. Identification of endogenous phospholipid ligands of $GABA_B$ receptor.

a,c, LC-MS/MS analysis of phospholipids bound to $GABA_B$ receptor (n=1). LC traces showing the abundance of PC 38:2 (**a**) and PE 38:5 (**c**) lipids in $GABA_B$ preparation relative to a CaS receptor control.

b,d, High-resolution MS spectra of the peaks in (**a, c**) (black) matched with standard spectra of PC 38:2 (**b**) and PE 38:5 (**d**) in red.

e,f, Molecular surface of $GABA_{B1b}$ (**e**) and $GABA_{B2}$ (**f**) TM domain showing the binding pocket for PE 38:5 and PC38:2, respectively.

g-j, Three views of the specific interactions between phospholipid and each $GABA_B$ subunit. Contacts are shown between the phospholipid head group and residues from $GABA_{B1b}$ (**g**) and $GABA_{B2}$ (**h**), as well as phospholipid fatty acyl chains and $GABA_{B1b}$ (**i**) and $GABA_{B2}$ (**j**).